Geosci. Model Dev. Discuss., 7, 5197–5248, 2014
www.geosci-model-dev-discuss.net/7/5197/2014/
doi:10.5194/gmdd-7-5197-2014


Geoscientific Model Development Discussions
Open Access



# Implementation and comparison of a suite of heat stress metrics within the Community Land Model version 4.5

**J. R. Buzan**[1,2], **K. Oleson**[3], **and M. Huber**[1,2]

[1]Department of Earth Sciences, University of New Hampshire, Durham New Hampshire, USA
[2]Earth Systems Research Center, Institute for Earth, Ocean, and Space Sciences, University of New Hampshire, Durham New Hampshire, USA
[3]National Center for Atmospheric Research, Boulder Colorado, USA

Received: 21 June 2014 – Accepted: 12 July 2014 – Published: 8 August 2014

Correspondence to: J. R. Buzan (jonathan.buzan@unh.edu)

Published by Copernicus Publications on behalf of the European Geosciences Union.

## Abstract

We implement and analyze 13 different metrics (4 moist thermodynamic quantities and 9 heat stress metrics) in the Community Land Model (CLM4.5), the land surface component of the Community Earth System Model (CESM). We call these routines the HumanIndexMod. These heat stress metrics embody three philosophical approaches: comfort, physiology, and empirically based algorithms. The metrics are directly connected to CLM4.5 BareGroundFuxesMod, CanopyFluxesMod, SlakeFluxesMod, and UrbanMod modules in order to differentiate between the distinct regimes even within one gridcell. This allows CLM4.5 to calculate the instantaneous heat stress at every model time step, for every land surface type, capturing all aspects of non-linearity in moisture-temperature covariance. Secondary modules for initialization and archiving are modified to generate the metrics as standard output. All of the metrics implemented depend on the covariance of near surface atmospheric variables: temperature, pressure, and humidity. Accurate wet bulb temperatures are critical for quantifying heat stress (used by 5 of the 9 heat stress metrics). Unfortunately, moist thermodynamic calculations for calculating accurate wet bulb temperatures are not in CLM4.5. To remedy this, we incorporated comprehensive water vapor calculations into CLM4.5. The three advantages of adding these metrics to CLM4.5 are (1) improved thermodynamic calculations within climate models, (2) quantifying human heat stress, and (3) that these metrics may be applied to other animals as well as industrial applications. Additionally, an offline version of the HumanIndexMod is available for applications with weather and climate datasets. Examples of such applications are the high temporal resolution CMIP5 archived data, weather and research forecasting models, CLM4.5 flux tower simulations (or other land surface model validation studies), and local weather station data analysis. To demonstrate the capabilities of the HumanIndexMod, we analyze the top 1 % of heat stress events from 1901–2010 at a 4× daily resolution from a global CLM4.5 simulation. We cross compare these events to the input moisture and temperature conditions, and with each metric. Our results show that heat stress may be

divided into two regimes: arid and non-arid. The highest heat stress values are in areas with strong convection (±30° latitude). Equatorial regions have low variability in heat stress values (±20° latitude). Arid regions have large variability in extreme heat stress as compared to the low latitudes.

## 1 Introduction

Heat death is the number one cause of death from natural disaster in the United States; more than tornados, flooding, and hurricanes combined (NOAAWatch, 2014). Short term duration (hours) of exposure to heat while working may increase the incidence of heat exhaustion and heat stroke (Liang et al., 2011). However, long term exposure (heat waves or seasonally high heat), even without working, may drastically increase morbidity and mortality (Kjellstrom et al., 2009). The 2003 European heat wave killed 40 000 people during a couple weeks in August (García-Herrera et al., 2010). The 2010 Russian heat wave, the worst recorded heat wave, killed 55 000 people over the midsummer (Barriopedro et al., 2011).

A growing literature is concerned with the frequency and duration of heat waves (Seneviratne et al., 2012 and references therein). One study concluded that intensification of 500 hPa height anomalies will produce more severe heat waves over Europe and North America in the future (Meehl and Tebaldi, 2004). Another study shows that even in the absence of El Ninos since 1997, there is increasing occurrence of extreme temperatures (Seneviratne et al., 2014). Multiple studies associate lack of precipitation and/or low soil moisture to contributing to high temperatures (Fischer et al., 2007; Mueller and Seneviratne, 2012; Miralles et al., 2014).

Regarding humans, however, temperature differences are not the primary method for heat dissipation. Evaporation of sweat is crucial to maintaining homeostasis, and none of the before mentioned studies incorporate atmospheric moisture to measure heat stress. Many different heat diagnostic indices were developed to diagnose heat stress (over a 100 year history, Table 1), such as the Wet Bulb Globe Temperature





GMDD
7, 5197–5248, 2014

(WBGT), the Discomfort Index (DI), or Heat Index (HI), and policy makers have decided to incorporate these indices in weather warning systems (Epstein and Moran, 2006; Parsons, 2006, 2013; Rothfusz, 1990; Fiala et al., 2011).

There are a limited number of studies validating, exploring, or using heat stress metrics on a global scale (Kjellstrom et al., 2009b; Hyatt et al., 2010; Sherwood and Huber, 2010; Fischer and Schar, 2010; Fischer et al., 2012; Fischer and Knutti, 2012; Willett and Sherwood, 2012; Dunne et al., 2013; Kjellstrom et al., 2013). Most of these studies do not capture the diurnal cycle of heat stress (Kjellstrom et al., 2009b; Hyatt et al., 2010; Fischer and Schar, 2010; Fischer and Knutti, 2012; Willett and Sherwood, 2012; Dunne et al., 2013; Kjellstrom et al., 2013), thus not representing both night time highs, and daytime extremes. For example, one study used monthly averages to calculate extreme heat stress (Dunne et al., 2013). Various forms of moist thermodynamic calculations (Buck, 1981; Davies-Jones, 2008; Stull, 2011) and heat stress metrics (ACSM, 1984) are criticized for their inaccuracies (Budd, 2008; Alfano et al., 2010; Davies-Jones, 2008). These calculations, however, are widely used (Sherwood and Huber, 2010; Hyatt et al., 2010; Fischer et al., 2012; Willett and Sherwood, 2012; Dunne et al., 2013; Kjellstrom et al., 2013). Occasionally, results using heat stress limits are misinterpreted. One study confuses wet bulb temperature thresholds with dry bulb temperature thresholds, which has misleading consequences (Benestad, 2010). Only one study includes solar radiation as a component in heat stress (Kjellstrom et al., 2013). Different metrics are used between each study, and no study attempts to compare more than two metrics.

Our goal here is to improve the situation by implementing and comparing a large suite of metrics, into a commonly used open source climate model, using the highest temporal variability and accurate moist thermodynamics we can bring to bear currently. This paper implements 13 different metrics into the Community Land Model (CLM4.5), a component model of the Community Earth System Model (CESM), maintained by the National Center for Atmospheric Research (NCAR) (Hurrell et al., 2013). The outline of the paper is as follows: Sect. 2 (Background) focuses on the development, calculation, and use of these 13 metrics. Section 3 (Methods) describes the implementation and model setup. Section 4 (Results) presents the results of a model simulation using these metrics. Section 5 (Discussion) discusses the implications of the research, and Sect. 6 (Summary) presents the conclusions of the paper.

## 2 Background

### 2.1 The structure of Community Land Model version 4.5

We use CLM version 4.5 which was released in June 2013. Boundary conditions for CLM4.5 consist of topography and atmospheric weather conditions. For example, CLM4.5 could be driven by other CMIP models output, or run in single grid cell mode configuration; the model is flexible. Each grid cell in CLM4.5 can include vegetation, lakes, wetlands, glacier, and urban. CLM4.5 includes a carbon-nitrogen cycle model that produces prognostic values of leaf and stem area and canopy height (Lawrence et al., 2011, 2012; Oleson et al., 2013a). Vegetation is discretized into 15 plant functional types (PFT), that may coexist in the same model grid cell (constituting a "biome"), consistent with ecological theory (Bonan et al., 2002). These biomes range from broadleaf evergreen trees to tundras. There are new parameterizations and models for snow cover, lakes, crops, and urban classifications (Oleson et al., 2013a). The urban biome, a single-layer canyon model, is designed to represent the "heat island", where temperatures are amplified by urban environments (Oleson et al., 2008a, b; Oleson et al., 2010a–c). The "heat island" effect can increase the likelihood of complications from human heat stress. Radiation is absorbed within the walls of the canyon, and air conditioners add waste heat to the local environment. Past CLM4 experiments have explored and contrasted temperatures between rural and urban environments (Oleson et al., 2011). The Oleson et al. (2011) present day experiment shows there is up to an annual difference of $\sim 4\,^{\circ}$C ($1.1\,^{\circ}$C on average) between the urban environment and local rural areas. These results are due in part to different partitioning





GMDD
7, 5197–5248, 2014

of latent and sensible heat fluxes compared to rural areas. For future scenarios with higher $CO_2$ concentrations, urban environments have substantially more hot days and warm nights than the present day (Oleson, 2012).

## 2.2 Thermodynamic water calculations

Humans dissipate ~ 75 % of their heat through the evaporation of sweat from their skin. Therefore, incorporating detailed and accurate calculations of water vapor in the atmosphere is a critical step for characterizing heat stress. Specifically, the potential to cool from evaporation is of particular interest, and is measured from wet bulb temperature. Wet bulb temperature ($T_w$) is the temperature an air parcel will cool to from evaporating water into that parcel until saturation. However, moist thermodynamic quantities, like $T_w$, are difficult to calculate efficiently. Decades of research has produced numerous methods of fast computations for $T_w$, but at the expense of accuracy. The more commonly used methods involve polynomial fits to Clausius–Clapeyron water vapor calculations (Wexler, 1976, 1977; Flatau et al., 1992), as in CLM4.5. Bolton's (1980) calculations were accurate, yet, wrestled with computational efficiency. 30 years have passed since Bolton's calculations, and 20 years since Flatau's polynomial fits. Computers have advanced in computational capabilities by orders of magnitude, and there are new methods for calculating $T_w$. There is a case for updating moist thermodynamical code within Earth system models.

The $T_w$ calculation we use (Davies-Jones, 2008) improves upon theory and previous calculation techniques (Bolton, 1980). Davies-Jones (2008) shows that the second order derivative of the equivalent potential temperature function (Eq. A20), with respect to $T_w$ and pressure, is a linear function from an interval of –20 °C–20 °C over the entire pressure range of the troposphere. Appendix A shows the Davies-Jones method. The accuracy of the first approximation allows the Newton–Raphson method (Eq. A22) to iterate once or twice before convergence. Thus, this process of calculating $T_w$ is computationally efficient and accurate.





GMDD
7, 5197–5248, 2014

An accurate calculation of $T_w$ is imperative for many metrics that are used for determining heat stress. Moist thermodynamical calculations are calculated in CLM4.5 through a module called QSatMod, using polynomial fits to vapor pressure calculations (Flatau et al., 1992). Unfortunately, Flatau's equations do not compute all the quantities necessary for calculating the Davies-Jones (2008) $T_w$ method. Specifically, the August–Roche–Magnus equation (ARM) (Eq. A13), which is used to calculate the derivative of the log of ARM (Eq. A15), is not part of Flatau's polynomials. Equation (A15) is required for Eq. (A9), a critical component for the initial guess of $T_w$ before applying the Newton–Raphson method. The ARM equation is valid over a similar range of pressures as Flatau's polynomials. The differences between ARM, its derivatives, and the polynomials are minor, with $< 1\,\%$ difference at $< 323$ K ($< 50\,^{\circ}$C) at 1000 mb (Fig. 1). Both ARM and Flatau's polynomials produce unrealistic saturation vapor pressure values $> 340$ K ($> 67\,^{\circ}$C) at 300 mb and at $> 360$ K ($> 87\,^{\circ}$C) at 1000 mb (Fig. 1). These unrealistic values are at temperatures that are not expected in modern, future, or paleo climates. The addition of ARM and its derivatives improves CLM4.5 by expanding the moist thermodynamical quantities available, while maintaining accuracy.

### 2.3 Heat stress modeling

The models for determining heat stress for humans vary greatly; ranging from simple indices to complex prognostic physiology modeling (Table 1). Prognostic human thermal models are beyond the scope of this paper, and instead, we are focusing on diagnostic indices. The diagnostic indices we chose all share common characteristics. Each index uses a combination of atmospheric variables: temperature ($T$), humidity ($Q$), and pressure ($P$). The different atmospheric variables are weighted dependent upon assumptions (such as local climate or the "average" human), and the experimental design that was used to create them. More complicated heat indices include components beyond the basic atmospheric state variables, such as radiation transfer and winds, accounting for convective fluxes, etc.





GMDD
7, 5197–5248, 2014

The primary focus of this work is on the atmospheric variable based metrics, not fluxes. Some of the more complicated atmospheric variable metrics include a function for wind (Apparent Temperature, see below), however, the majority of the metrics we use implicitly include winds. Note that most of these metrics have units of temperature, which can be misleading. The metrics have temperature scales for comparative purposes only, as the metrics are an index, not a true thermodynamic quantity. We break these metrics into three categories, based upon design philosophies: comfort, physiological response, and empirical fit. Comfort based algorithms are a quantification of behavioral or "feels like" reactions to heat in both animals and humans. Physiological indices quantify the physical response mechanisms within a human or animal, such as changes in heart rate or core temperature. The empirical indices quantify relationships between weather conditions and a non-physical or comfort related attribute. For example, a empirical algorithm's result may determine how much work may be completed per hour per weather condition. The following sections describe algorithms commonly used for diagnosing heat stress (see variables defined in Table 2).

#### 2.3.1 Comfort algorithms

The underlying philosophical approach to deriving comfort metrics is representing behavioral reactions to levels of comfort (Masterson and Richardson, 1979; Steadman, 1979a). The goal of these equations of comfort is to match the levels of discomfort to appropriate warnings for laborers (Gagge et al., 1972) and livestock (Renaudeau et al., 2012). Discomfort in humans sets in much earlier than actual physiological responses, i.e. the human body provides an early warning to the mind that continuing the activity may lead to disastrous consequences. For example, when heat exhaustion sets in, the body is sweating profusely, and often there are symptoms of dizziness. However, the actual core temperature for heat exhaustion is defined at 38.5 °C, which is considerably lower than heat stroke (42 °C). Apparent Temperature, Heat Index, Humidex, and Temperature Humidity Index account for the comfort level, and they were tailored to





GMDD
7, 5197–5248, 2014

the world locations where they were developed in, or streamlined for ease of use, as described further below.

Apparent Temperature (AT) was developed using a combination of wind, radiation, and heat transfer to measure thermal comfort and thermal responses in humans (Steadman, 1994). AT is used by the Australian Bureau of Meteorology, and was developed for climates in Australia (ABM, 2014). The metric is an approximation of a prognostic thermal model of human comfort (Steadman, 1979a, b; Steadman, 1984), and is as follows:

$$\mathrm{AT} = T_\mathrm{c} + \frac{3.3 e_\mathrm{RH}}{1000} - 0.7 u_{10\mathrm{m}} - 4 \tag{1}$$

$$e_\mathrm{RH} = \left(\mathrm{RH}/100\right) e_\mathrm{sPa} \tag{2}$$

where vapour and saturated vapour pressures ($e_\mathrm{RH}$ and $e_\mathrm{sPa}$, respectively), are in Pascals. $u_{10\mathrm{m}}$ ($\mathrm{m\,s^{-1}}$) is the wind velocity measured at 10 m height. Air temperature ($T_\mathrm{c}$) and AT are in °C. RH (%) is the relative humidity. Of the metrics we implement, this is the only metric that includes wind velocity explicitly; the others assume a reference wind. An assumption for AT is that the subject is outside, but not exposed to direct sunlight. AT has no explicit thresholds, rather the index shows an amplification of temperatures. Previous work, however, has used temperature percentiles to describe AT (Oleson et al., 2013b).

Heat Index (HI) was developed using a similar process as AT. The United States National Weather Service (NWS) required a heat stress early warning system, and the index was created as a polynomial fit to Steadman's (1979a) comfort model.

$$\begin{aligned}\mathrm{HI} = &-42.379 + 2.04901523 T_\mathrm{f} + 10.14333127\mathrm{RH} + -0.22475541 T_\mathrm{f}\mathrm{RH} + -6.83783 \\ &\times 10^{-3} T_\mathrm{f}^2 + -5.481717 \times 10^{-2}\mathrm{RH}^2 + 1.22874 \times 10^{-3} T_\mathrm{f}^2\mathrm{RH} + 8.5282 \\ &\times 10^{-4} T_\mathrm{f}\mathrm{RH}^2 + -1.99 \times 10^{-6} T_\mathrm{f}^2\mathrm{RH}^2\end{aligned} \tag{3}$$

Here, air temperature ($T_\mathrm{f}$) and HI are in Fahrenheit, and RH is as described previously. HI has a number of assumptions. The equation assumes a walking person in shorts and





GMDD
7, 5197–5248, 2014

T-shirt, who is male and weighs ∼ 147 lbs (Rothfusz, 1990). Additionally, this subject is not in direct sunlight. As with AT, HI represents a "feels like" temperature, based upon levels of discomfort. HI uses a scale for determining heat stress: 27–32 °C is caution, 33–39 °C is extreme caution, 40–51 °C is danger, and ≥ 52 °C is extreme danger.

Humidex (HUMIDEX) was developed for the Meteorological Service of Canada, and describes the "feels like" temperature for humans (Masterson and Richardson, 1979). The original equation used dew point temperature, rather than specific humidity. The equation was modified to use vapour pressure, instead:

$$\mathrm{HUMIDEX} = T_c + \frac{5}{9}\left(\frac{e_{RH}}{100} - 10\right) \quad (4)$$

where air temperature ($T_c$) and vapor pressure ($e_{RH}$) are as described previously, and HUMIDEX is unitless, because the authors recognized that the index is a measure of heat load. The warning system has a series of thresholds: 30 is some discomfort, 46 is dangerous, and 54 is imminent heat stroke.

The Temperature Humidity Index for Comfort (THIC) is a modification of the Temperature Humidity Index (THI) (Ingram, 1965). Comfort was quantified for both humans and livestock through THIC (NWSCR, 1976), however, we use a calibration for pigs. The index is unitless:

$$\mathrm{THIC} = 0.72T_w + 0.72T_c + 40.6 \quad (5)$$

where $T_w$ is in units of Celsius. The index is used to describe behavioral changes in large animals due to discomfort (seeking shade, submerging in mud, etc.). The index is in active use by the livestock industry for local heat stress and future climate considerations (Lucas et al., 2000; Renaudeau et al., 2012). The index describes qualitative threat levels for animals: 75 is alert, 79–83 is dangerous, and 84+ is very dangerous. There are different approaches to the development of THIC, including considerations of physiology of large animals.





GMDD
7, 5197–5248, 2014

### 2.3.2 Physiology algorithms

Numerous metrics are based upon direct physiological responses within humans and animals, however, almost all of them are complicated algorithms (e.g. Moran et al., 2001; Berglund and Yokota, 2005; Gribox et al., 2008; Maloney and Forbes, 2011; Havenith et al., 2011; Gonzalez et al., 2012; Chan et al., 2012). The Universal Thermal Climate Index (UTCI) was developed to determine human heat stress through biometeorology (Bröde et al., 2012; Fiala et al., 2011; Havenith et al., 2011), with the intention of integration into weather prediction and climate models (Jendritzky et al., 2009). The effort failed to couple the prognostic thermal model of humans into weather and Earth system model framework, however, the UTCI was the resulting product (Bröde et al., 2013). The index is a polynomial fit to an ensemble of simulations of weather effects on humans with inputs being dry bulb, wet bulb, and radiation temperatures. This metric, along with many other physiological based metrics requires radiation measurements, or heart rates, or even sweat rates. We are not using metrics that include wind, radiation, etc., because metrics that use $T$, $P$ and $Q$ are in common use. The available metrics that are calibrated for physiological responses using only meteorological inputs, though, are limited.

The Temperature Humidity Index for Physiology (THIP) is one such metric:

$$\mathrm{THIP} = 0.63T_\mathrm{w} + 1.17T_\mathrm{c} + 32 \tag{6}$$

where the temperature inputs are the same as in Eq. (5) (Ingram, 1965). THIP and THIC are generalized by the format:

$$\mathrm{THI} = aT_\mathrm{w} + bT_\mathrm{c} + c \tag{7}$$

where the constants $a$, $b$, and $c$ (not to be confused with variables in equations from Appendix A) are adjusted for the particular livestock animal. These constants are based upon physiology or comfort (Lucas et al., 2000). THIP is derived from core temperatures of large animals. Both THIP and THIC use the same scale for determining





GMDD
7, 5197–5248, 2014

qualitative threat levels. Additionally, THIC and THIP have applications beyond heat stress. THIP and THIC threshold levels are computed from both indoor and outdoor atmospheric variables. The differences between outdoor and indoor values are used to evaluate evaporative cooling mechanisms, e.g. swamp coolers (Gates et al., 1991a, b).

### 2.3.3 Empirical algorithms

The third category of algorithms is derived from first principle physical models of thermal regulation, changes in work loads, etc., and are then reduced to an empirical fit. Many empirically based algorithms are used for measuring heat stress indirectly, such as swamp cooler efficiency. Like the physiology based indices, many empirical algorithms involve metrics beyond atmospheric variables. These simplified versions are widely used, however, their accuracy is questionable. For example, natural wet bulb temperature (Brake, 2001) – dependent on radiation transfer, wind speed, and evaporation – can have up to three different values in the same convective environments (Alfano et al., 2012). We chose atmospheric variable heat stress metrics that do not have multiple end-members. These metrics either use the Davies-Jones (2008) $T_w$, or have eliminated the end-member issue through their empirical algorithms.

Two commonly used metrics that are widely used, but not verified, are the Simplified Wet Bulb Globe Temperature (sWBGT) and Indoor Wet Bulb Globe Temperature (indoorWBGT). sWBGT is based upon the Wet Bulb Globe Temperature (WBGT) that was developed as a decision making tool for the United States Marine Corps to mitigate heat stress casualties during training (Minard et al., 1957). The WBGT uses a combination of wet bulb and dry bulb temperatures as well as a globe thermometer ($T_g$).

$$\mathrm{WBGT} = 0.7T_w + 0.2T_g + 0.1T_c \tag{8}$$

$T_g$ is a black painted copper globe with a thermometer placed at the center, and measures a combination of radiation and advection temperatures (Keuhn et al., 1970; Liljegren et al., 2008). Due to the complicated nature of calculating/measuring $T_w$ and $T_g$

(~ 30 min for the $T_g$ to reach equilibrium), indoorWBGT removes $T_g$ and sWBGT does away with both $T_w$ and $T_g$ entirely.

$$\text{indoorWBGT} = 0.7T_w + 0.3T_c \tag{9}$$

$$\text{sWBGT} = 0.56T_c + \frac{0.393e_{RH}}{100} + 3.94 \tag{10}$$

sWBGT was designed for estimating heat stress in sports medicine, adopted by the Australian Bureau of Meteorology, and is acknowledged that its accuracy may be questionable (ABOM, 2010; ACSM, 1984; ACSM, 1987). We did not implement WBGT, nor indoorWBGT. WBGT requires radiation, and is outside the scope of this work. indoorWBGT is criticized explicitly for no recalibration due to removing radiation (Budd, 2008). We chose, however, to implement sWBGT due to its wide use. sWBGT is unitless, and its threat levels are: 26.7–29.3 is green or be alert, 29.4–31.0 is yellow or caution, 31.1–32.1 is red or potentially dangerous, and ≥ 32.2 is black or dangerous conditions (US Army, 2003).

Discomfort Index (DI) has had a similar development history as the WBGT. Developed in the 1950s as a calibration for air conditioners (Thom, 1959), it was adapted by the Israeli Defense Force as a decision making tool regarding heat stress (Epstein and Moran, 2006). DI requires $T_w$ and $T_c$. The computation of $T_w$ in the past was difficult, and the DI equations often used approximations (Oleson et al., 2013b):

$$T_{wS} = T_c \arctan\left(0.151977\sqrt{RH + 8.313659}\right) + \arctan(T_c + RH) - \arctan(RH - 1.676331) + 0.00391838RH^{3/2}\arctan(0.023101RH) - 4.68035 \tag{11}$$

where $T_{wS}$ is the wet bulb temperature in Celsius (Stull, 2011). Stull's function has limited range of effective accuracy.

$$\frac{-20 < T_c < 50}{-2.27T_c + 27.7 < RH < 99} \tag{12}$$





GMDD
7, 5197–5248, 2014

where, not only is the function dependent on RH, but also a function of $T_c$. DI is calculated from these inputs:

$$DI = 0.5T_w + 0.5T_c \quad (13)$$

where the DI is unitless. We compute DI with both $T_{wS}$ and $T_w$. We keep the legacy version (Stull, 2011) for comparative purposes. The index is unitless, and the warning levels are indicator of threats to the populations: 21–24 is < 50 % of population in discomfort, 24–27 > 50 % of population in discomfort, 27–29 most of the population in discomfort, 29–32 severe stress, and > 32 is state of emergency (Giles et al., 1990).

The last index we present is a measurement of the capacity of evaporative cooling mechanisms. Often, these are referred to as swamp coolers. Large scale swamp coolers generally work by spraying a "mist" into the air, or blowing air through a wet mesh. This mist then comes in contact with the skin, and subsequently evaporated, thus cooling down the subject. In dry environments, they can be an effective mass cooling mechanism. Unfortunately, swamp coolers raise the local humidity considerably, reducing the effectiveness of direct evaporation from the skin. Swamp coolers are measured by their efficiency:

$$\eta = \frac{T_c - T_t}{T_c - T_w} 100\,\% \quad (14)$$

where $\eta$ (%) is the efficiency, and $T_t$ is the target temperature for the room to be cooled towards in Celsius (Koca et al., 1991). Rearranging Eq. (14) and solving for $T_t$:

$$T_t = T_c - \frac{\eta}{100}(T_c - T_w) \quad (15)$$

where $T_t$ is now the predicted temperature based upon environmental variables. The maximum efficiency of typical swamp coolers is 80 %, and a typical value of a substandard mechanism is 65 % (Koca et al., 1991). Thus, we calculate $T_t$ with two different efficiencies: SWMP80, for $\eta$ at 80 %, and SWMP65 for $\eta$ at 65 %. With the mist injected air cooled to $T_t$, $T_t$ is approximately equal to a new local $T_w$. Humid environments or environments that are hot and have an above average RH relative to their normally high $T$, severely limit the cooling potential of swamp coolers. The livestock industry uses evaporative cooling mechanisms for cooling, and often in conjunction with THIP and THIC, as mentioned previously (Gates et al., 1991a, b). Due to their low cost, swamp coolers are used throughout the world as a method of cooling buildings and houses. No one has implemented SWMP65 and SWMP80 in global models, and we believe that this will provide many uses to industry by its inclusion in CLM4.5. Table 2 shows what metrics are discussed in this paper.

## 3 Heat stress modeling

Our approach is to choose a subset of heat stress metrics that are in common use operationally by governments and/or used extensively in prior climate modeling studies (Table 3). We do this in order to provide a framework to allow comparisons of metrics across studies, and we designate the algorithms the HumanIndexMod. Section 3.1 discusses the implementation of the HumanIndexMod into CLM4.5. Section 3.2 describes our simulation setup that we use to demonstrate the capabilities of the HumanIndexMod. The simulation is for showcasing the HumanIndexMod, not as an experiment for describing real climate or climate change. Section 3.3 describes a unique application method for analyzing heat stress.

### 3.1 HumanIndexMod design and implementation

There are two philosophical aspects to the design of the HumanIndexMod. (1) the improvement of thermodynamic quantities regarding water, and (2) a modular format to increase use through both narrowly focused applications and up to broad based studies. The module is in an open source format, and is incorporated into the CLM4.5 developer branch (the module itself is available from the corresponding author). The modular format encourages adapting the code to specific needs; whether that focus is on improving water vapor calculations or heat stress. The inclusion of heat stress metrics covering comfort, physiology, and empirical philosophies encourages the use of HumanIndexMod for many applications.

We directly implemented the code into the CLM4.5 architecture through seven modules. Four of these modules – BareGroundFuxesMod, CanopyFluxesMod, SlakeFluxesMod, and UrbanMod – call the HumanIndexMod. The HumanIndexMod is calculated for every surface type in CLM4.5. The design of CLM4.5 allows the urban and rural components, where the rural component represents the natural vegetation surface, to be archived separately for intercomparison. The HumanIndexMod uses the 2 m calculations of water vapor, temperature, and pressure, as well as 10 m winds. Three other modules are modified with the implementation process. These modules – clmtype, clmtypeInitMod, and histFldsMod – are used for initializing memory and outputting variable history files.

As previously mentioned in Sect. 2.2, moist thermodynamic water vapor quantities in CLM4.5 are calculated within QSatMod. We use the outputs from QSatMod as the inputs to the HumanIndexMod. Within the HumanIndexMod, we created a subroutine, QSat_2, that has all the same functionalities as QSatMod. These algorithms calculate $T_w$ using Davies-Jones (2008). We show acceptable differences between QSatMod and QSat_2, previously mentioned in Sect. 2.2 (Fig. 1). This subroutine uses the ARM equation, calculates $f(\theta_E)$ (Eq. A18) with respect to the input temperature, and the subsequent derivatives. The new subroutines improve CLM4.5 by calculating previously uncalculated thermodynamic quantites, thus creating new opportunities for future researchers to replace QSatMod with QSat_2.

We implement all of the thermodynamic routines developed by Davies-Jones (2008) (see Appendix A). Equation (A.4) is the most accurate and efficient $\theta_E$ calculation available (Bolton, 1980; Davies-Jones, 2009). Calculating Eq. (A4) required implementing $T_L$ and $\theta_{DL}$ (Eqs. A2 and A3, respectively) into the HumanIndexMod. $T$, $P$, and $Q$ from CLM4.5 are used to calculate $\theta_E$ and $T_E$ (Eq. A5). $T_E$ is the input into QSat_2 for calculating the initial guess of $T_w$, and subsequently followed by the Newton–Raphson method (Eqs. A9–A22). We found it advantageous to split the heat stress quantities into their own subroutines, allowing the user to choose what quantities to be calculated. The minimum requirements to execute the entire module are $T$ (K), $P$ (Pa), RH (%), $Q$ ($\mathrm{g\,kg^{-1}}$), $e$ (Pa), and $u_{10m}$ ($\mathrm{m\,s^{-1}}$). Table 4 shows the subroutines, input requirements, and outputs in HumanIndexMod.

### 3.2 CLM4.5 experimental setup

CLM4.5 may be executed independently of the other models in CESM, called an I-Compset. To do so, CLM4.5 requires atmospheric boundary conditions. We use the default dataset for CLM4.5 – CRUNCEP. CRUNCEP is the NCEP/NCAR reanalysis product (Kalnay et al., 1996) corrected and downscaled by the Climatic Research Unit (CRU) gridded observations dataset from the University of East Anglia (Mitchell and Jones, 2005). The time period is 4× daily from 1901–2010, and is on a regular grid of $\sim 0.5^\circ \times 0.5^\circ$. The combination of CRU and NCEP products was to correct for biases in the reanalysis product, and improve overall resolution (Casado et al., 2013). To drive CLM4.5 we used surface solar radiation, surface precipitation rate, temperature, specific humidity, zonal and meridional winds, and surface pressure.

CLM4.5 was released in June 2013, and the model has substantial improvements over previous versions – including improved urban canyon components, as well as new biogeochemical cycles (Oleson et al., 2013a). Our simulation has the carbon and nitrogen cycling on (biogeophysics “CN”). The simulation has the HumanIndexMod included. The simulation was initialized at year 1850, on a finite volume grid of $1^\circ \times 1^\circ$, using boundary conditions provided from NCAR (Sam Levis, personal communication). The simulation spun up while cycling 3 times over CRUNCEP 1901–1920 forcings. Once completed, our experiment used the spun up land conditions, and ran the entirety of 1901–2010.





GMDD
7, 5197–5248, 2014

### 3.3 Heat stress indices analysis

We outputted 4× daily averages of the heat stress metrics and the corresponding surface pressure ($P$), 2 m temperature ($T$), 10 m winds ($u_{10m}$), and 2 m humidity ($Q$) fields. The 4x daily files are compiled into yearly files with 1460 time steps, and a concatenated file from 1901–2010. We computed statistics for the time series (mean, variance, exceedance, etc.). We focus on the 99th percentiles (hottest 1606 six hour intervals, ∼ 402 days).

The 99th percentile between different heat stress metrics may not involve the same $T$, $P$, and $Q$ combinations. To quantify these differences requires analyzing the original inputs used to calculate the heat stress metric. Every 6 h period within the 99th percentiles were located within the time series, and we calculated the joint distribution. For example, the 99th percentile of HI isolated the top 1606 hottest time steps in each latitude by longitude. After calculating the joint distribution, we use the time domain to isolate all other quantities, allowing cross comparison between all metrics and HI. The goal was to develop an analysis technique comparing all heat stress metrics within CLM4.5.

After the joint distributions are calculated, we, again, compute the statistical dispersion (mean, variance, exceedance, etc.) of the 99th percentiles. We developed two methods of displaying the output for visual analysis with maps and point comparisons. These maps are the 99th percentiles of the metrics and the medians of their joint distribution. We selected a variety of regional city localities around the world to demonstrate latitudinal and regional influences on heat stress (Table 5). These locations were chosen due to high concentrations of people, or unique environments (i.e. deserts, coastal, monsoons, etc.). Due to the variance that an individual grid cell may have, we averaged the statistical dispersion (mean, variance, exceedance, etc.) information of all 8 nearest local grid cells together. We plotted the joint distributions as box and whisker diagrams. The 25th and 75th percentiles are the box edges, the median as the horizontal bar, the lower whisker as 5th, and the 90th as the upper whisker (the upper tail is discussed in

Sect. 5). The following section displays some of the results and their characterization within CLM4.5.

## 4 Results

We present a snap shot of the many metrics calculated. We show an example of the possible global applications for these metrics. Additionally, we break down the analysis into two sections: joint distribution maps and box plots. This approach characterizes heat stress within CLM4.5 in response to one observation reanalysis product, the CRUNCEP.

### 4.1 Joint distribution maps

We present 1901–2010 99th percentile joint distributions maps of $Q$, $T$, $T_w$, $\theta_E$, and the heat stress metrics, HI, sWBGT, SWMP65, and SWMP80 (Figs. 2 and 3). The figures and text use the labeling convention "B_g_A" (metric "B" given metric "A"), and this is the joint distribution displayed. $T_w$ maximums appear in central South America, Western Africa, the Arabian Pennisula, north-western Australia, and Northern India/Pakistan (Fig. 2g). sWBGT, HI, SWMP65, SWMP80, and $\theta_E$ (Eq. A4) (Figs. 2a, d, 3a, d, and g, respectively) have their global maximums in the same locations as this maximum $T_w$. The spatial distribution of maximums in $T_w$ and $\theta_E$ are nearly identical (Figs. 2g and 3g). This is unsurprising given their underlying similarity as a buoyancy measure. The spatial distribution of heat stress metrics is nearly the same with regional differences, which become apparent in the joint distributions of $T$ and $Q$.

The joint distributions of the thermodynamic variables and heat stress tease apart the subtle differences in the spatial distributions of heat stress. HI shows that the dominant contributor to the metric is high $T$ (Fig. 2e), while $Q$ in the low latitudes is not as strong of a contributing factor (Fig. 2f). Globally, 99th percentiles of $T_w$ and $\theta_E$ correspond to the local 99th percentiles of $Q$ (Figs. 2i and 3i). Where global maximums of heat stress





GMDD
7, 5197–5248, 2014

occur, they match $T_w$, as mentioned in the previous paragraph, and are all in locations of high $Q$. In high latitudes, all metrics follow maximum $T$ and $Q$ equally. The joint distributions of SWMP65 and SWMP80 with $T$ and $Q$ differ subtly (Fig. 3b, c, e, and f). These differences become apparent when compared to other heat stress metrics. For example, inefficient evaporative cooling mechanisms (SWMP65) spatially vary as HI (Figs. 2e, f, and 3b, c). Whereas, efficient evaporative cooling mechanisms (SWMP80) spatially vary closer to sWBGT and $T_w$. (Figs. 2b, c, h, i and 3e, f). We discuss the potential meaning of this result in Sect. 5.2. We have analyzed the median values of the joint distributions spatially. However, to characterize why the regional spatial patterns vary, we need to look at the full distribution of the values. To do this, we look into the regional variations with box plots.

## 4.2 Joint distribution box plots

We examine regional differences between heat stress and thermodynamic quantities. The variability of the extremes in heat stress is dependent on regional location. To simplify the regional analysis, we focus on areas of the world where humans live in large concentrations, i.e. metropolitan locations (Table 5). We also chose these locations because of frequent exposure to heat stress, or because they have recently experienced extreme heat events. Additionally, these localities are grouped by 4 climatological similarities: moist convective (red), equatorial (blue), arid (grey), and mid-latitude (green). We display two sets of joint distributions; one set is the absolute value comparisons, and the second determines what part of the climatology that the joint variable originates from. We split the joint distribution plots into 4 panels: 2 panels show $T$ and $Q$ absolute value variations (Figs. 4 and 6, respectively), and 2 panels show $T$ and $Q$ time series percentiles (Figs. 5 and 7, respectively).

The magnitudes of $T$ in maximum heat stress may vary up to 5 °C (Fig. 4), whereas the heat stress metrics vary much less (1–2 °C) (not shown). All of the metrics show that the hottest heat stress values occur where there is the highest $Q$ – the convective and equatorial regions (Fig. 6). Equatorial regions have both low variability in $T$ and





GMDD
7, 5197–5248, 2014

$Q$ when compared to other regions (Figs. 4 and 6). There are two regimes of heat stress: arid (grey), and non-arid (coloured). The arid regions have higher $T$ and lower $Q$ than the non-arid regions, which is reasonable due to less precipitation and/or water availability. In the arid regions, $Q$ has low median values, and an extremely long tail (Fig. 6). We do not believe these tail values are reasonable (see Sect. 5).

The time series percentiles (Figs. 5 and 7) show that although absolute magnitudes of both $T$ and $Q$ drop off with latitude, the maximum heat stress is tied to the top $T$ and $Q$, locally. Except for a few instances, all 99th percentile heat events draw upon at least the 80th percentile in both $T$ and $Q$. As $T_w$ and $\theta_E$ approach their global maximum values, the distribution of $Q$ approaches the 99th (Fig. 7c and e, respectively). Both sWBGT and SWMP80 show similar patterns to $T_w$ (Fig. 7a and f, respectively). The converse applies to $T$ for sWBGT, $T_w$, $\theta_E$ and SWMP80 (Fig. 5a, c, e, and f). As mentioned in Sect. 4.1, HI and SWMP65 have the similar features that are dissimilar to the other quantities (Figs. 5b, d and 7b, d, respectively) (see Sect. 5.2).

## 5 Discussion

We designed the HumanIndexMod to calculate diagnostic heat stress and moist thermodynamics systematically. There are many approaches to evaluating heat stress. Monthly and seasonal temperature and moisture averages were used for general applications (Diffenbaugh et al., 2007; Dunne et al., 2013), however these averages underestimate the potential severity of heat stress (not shown). This is due to the non-linear covariance of $T$ and $Q$, and monthly averages miss the extremes. Recent research used daily values (Kjellstrom et al., 2009b; Hyatt et al., 2010), but ultimately, capturing the diurnal cycle is crucial for quantifying heat stress extremes (Oleson et al., 2013b). Heat stress related illness is exacerbated by high heat stress nights as well as daytime. To accurately calculate these extremes, one needs either high temporal resolution data, or by directly computing them at each time step within climate models. We discuss the results from the implementation separately: moist thermodynamics and heat stress.





GMDD
7, 5197–5248, 2014

## 5.1 Moist thermodynamics

The HumanIndexMod has applications beyond just human heat stress. For example, these metrics maybe used as a model diagnostic. The high $Q$ values in the arid regions appear to be unreasonable because their absolute maximum $T_w$ are equivalent to the values found in the centers of hurricanes (Zhang et al., 2002; Smith and Montgomery, 2012) (we omit those CLM4.5 values in our results with the top whisker limited to the 90th percentile). Upon further analysis, we believe there are two reasons. (1) the BareGroundFuxesMod fluxes are calculated at the surface, not at 2 m height as with the CanopyFluxesMod, SlakeFluxesMod, and UrbanMod modules. This could cause high anomalous water quantities to be interpolated to the 2 m height. (2) the sand parameterizations are based upon Southwestern United States deserts (Brooks and Corey, 1964; van Genuchten, 1980), which are hard calcretes, not loose sands as many deserts are around the world. This causes pooling of water from an extreme rainfall event on the surface. The pooled water creates saturated vapor pressure values at high temperatures that are then interpolated to the 2 m height. This inflates $T_w$ to unreasonable numbers. There is a possibility that this issue is linked to a long standing issue with simulating monsoons in desert regions (Meehl et al., 2006; Cook et al., 2012). This is just one way to take thermodynamic metrics beyond human heat stress to diagnose climate models.

## 5.2 Heat stress

We show that there are two regimes of heat stress globally – arid and non-arid. The arid regions consistently have higher temperatures and lower humidities than the non-arid areas. However, we show that maximum heat stress is tied to maximum $T$ and $Q$ globally. Characterizing arid regions vs. non-arid regions may require different heat stress metrics (e.g. Oleson el al., 2013b, specifically the comparison between Phoenix and Houston). The HumanIndexMod provides this capability.





GMDD
7, 5197–5248, 2014

The features of high heat stress are robust between model versions (Oleson et al., 2011; Fischer et al., 2012; Oleson et al., 2013b). Using heat stress metrics in Earth system modeling inherently reduces the uncertainties of climate change. Due to the conservation of energy and entropy, calculating heat stress shows that climate models and reanalysis fall along constant lines of $T_E$, even out to the 99th percentile (Fischer and Knutti, 2012). Previous modeling studies have demonstrated that urban equatorial regions transition to a nearly permanent high heat stress environment when considering global warming (Fischer et al., 2012; Oleson et al., 2013b). The convective regions (Fig. 4, red) are areas with the highest heat stress maximums and are often near coastal locations. Many of these metropolitan areas are in monsoonal regions which have strong yearly moisture variability. Heat stress in both equatorial and monsoonal regions is expected to increase dramatically when considering global warming (Kjellstrom et al., 2009b; Fischer and Knutti, 2012; Dunne et al., 2013; Oleson et al., 2013b). Accurate calculations from the HumanIndexMod will aid future characterizations of heat stress.

Calculating multiple heat stress metrics at every time step within climate models opens up avenues of research that were previously intractable due to insufficient data storage capabilities for high temporal resolution variables. We show that SWMP65 and SWMP80 diverge in their values (Fig. 5d, f and 7d, f, respectively). SWMP80 and sWBGT are similar in patterns with $T_w$ while HI and SWMP65 have similar patterns. These relationships may be related to the assumptions that were used to derive sWBGT and HI. WBGT, where sWBGT was derived from, was calibrated for US Marine Corps Marines (Minard et al., 1957), who are in top physical condition. HI was calibrated for an "average" American male (Steadman, 1979a; Rothfusz, 1990). This is similar to a circuit resistor, or stomatal resistance (Oke, 1987), which is measure of efficiency. The "average" person may be acting as a stronger resistor to evaporation than one that is acclimatized. An avenue of research that may be explored through climate modeling using the HumanIndexMod is the effects of acclimatization, and its impact on efficiency of evaporative cooling.





GMDD
7, 5197–5248, 2014

Exposure to high moist temperatures, ultimately, threatens humans physically, and long term exposure may lead to death. Extreme moist temperatures are projected to increase in the future, and potentially may reach deadly extremes, permanently in some regions (Sherwood and Huber, 2010). Heat stress indices have the ability to diagnose instantaneous exposure. Evaluating the potential impacts of long term exposure to heat stress, however, cannot be measured accurately by diagnostic models. Prognostic thermal physiological models can be used to predict the complexities of heat stress on humans.

Prognostic thermal physiology considers wind, ambient temperature, and moisture from the environment, as well as internal processes, such as blood flow and sweat. There are numerous different forms of prognostic models (Table 1). Some of them are quite complicated, using hundreds of grid cells to represent all parts of the body (Fiala et al., 1999). Less complicated models represent the human body as a single cylinder with multiple layers (Kraning and Gonzalez, 1997). Neither computational method is currently coupled to Earth system models, and this is a significant gap in determining future heat stress impacts that the HumanIndexMod may not be able to fulfill. To make progress towards representing the effects of heat stress on the human body prognostically, we recommend, as a first step, incorporating mean radiant temperature of humans. Radiation is a major component of human energy balance, and implementing this also allows incorporating more accurate diagnostics, such as WBGT and UTCI.

## 6 Summary

We present the HumanIndexMod that calculates 9 heat stress metrics and 4 moist thermodynamical quantities. The moist thermodynamic variables use the latest accurate and efficient algorithms available. The heat stress metrics cover three developmental philosophies: comfort, physiological, and empirically based algorithms. The code is designed, with minimal effort, to be implemented into general circulation, land surface,





GMDD
7, 5197–5248, 2014

and weather forecasting models. Additionally, this code may be used with archived data formats and local weather stations.

Furthermore, we have implemented the HumanIndexMod into the latest public release version of CLM4.5. We show that the module may be used to explore new avenues of research: characterization of human heat stress, model diagnostics, and intercomparisons of heat stress metrics. Our results show that there are two regimes of heat stress, arid and non-arid, yet all extreme heat stress is tied to maximum temperatures with maximum moisture.

Our approach has limitations. None of the metrics in the HumanIndexMod include the effects of solar and thermal radiation. Radiation is a non-negligible component of heat stress. As a consequence, the heat stress metrics presented always assume that the subject is not in direct solar exposure. Additionally, the indices represent a diagnostic environment for heat stress. These metrics do not incorporate prognostic components or complex physiology of the human thermal system.

Overall, the HumanIndexMod provides a systematic way for implementing an aspect of thermo-animal physiology into an Earth system modeling framework. Incorporating the HumanIndexMod into a variety of different models would provide a baseline for model-model comparisons of heat stress, such as the Coupled Model Intercomparison Project (CMIP) (Taylor et al., 2012) and other collaborative modeling frameworks. We encourage researchers to incorporate the HumanIndexMod within their research environments.

## Appendix A: Moist thermodynamics

We introduce terminology to describe the Davies-Jones (2008) calculation. All temperature subscripts that are capitalized are in Kelvin, while lower case are in Celsius. $\kappa_d$ is the Poisson constant for dry air (0.2854), and $\lambda$ is the inverse (3.504). Many of the following equations are scaled using non-dimensional pressure (also known as the Exner





GMDD
7, 5197–5248, 2014

function), $\pi$:

$$\pi = \left(p/p_0\right)^{1/\lambda} \tag{A1}$$

where $p$ is the pressure (mb), and $p_0$ is a reference pressure (1000 mb).

To define $T_\text{w}$ (the wet bulb temperature), we solve for the equivalent potential temperature, $\theta_\text{E}$. Determining $\theta_\text{E}$ is a three step process. First, we solve for the lifting condensation temperature ($T_\text{L}$):

$$T_\text{L} = \frac{1}{\frac{1}{T-55} - \frac{\ln\left(\text{RH}/100\right)}{2840}} + 55 \tag{A2}$$

where $T$ is the parcel temperature (Kelvin). For example, we use the 2 m air temperature in CLM4.5. RH (%) is taken at the same height as $T$. $T_\text{L}$ (Eq. A2), from Eq. (22) Bolton (1980), is the temperature at which a parcel that is lifted, following a dry adiabatic lapse rate, begins to condense. Second, as the air rises further, the parcel now follows a moist potential temperature, $\theta_\text{DL}$:

$$\theta_\text{DL} = T\left(\frac{p_0}{p-e}\right)^{\kappa_\text{d}}\left(\frac{T}{T_\text{L}}\right)^{0.00028r} \tag{A3}$$

where $e$ is the parcel vapor pressure (mb) (using CLM4.5, this is the 2 m vapor pressure), and $r$ is the mixing ratio (g kg$^{-1}$) (this is converted from the 2 m height $Q$ to $r$ in CLM4.5). Third, the parcel is raised to a great height where all latent heat is transferred to the air parcel, and the water is rained out, giving the solution to $\theta_\text{E}$. There are many methods for representing this process. The analytical solution (Holton, 1972) is computationally prohibitive in atmospheric and land surface models. There are various approximations of different aspects of potential and saturated temperatures to calculate $\theta_\text{E}$ (Betts and Dugan, 1973; Simpson, 1978), however, many of them have large errors. These errors are compared in Bolton (1980), and Eq. (39) (Bolton's formulation)





GMDD
7, 5197–5248, 2014

is up to an order of magnitude more accurate:

$$\theta_E = \theta_{DL} \exp\left[\left(\frac{3.036}{T_L} - 0.001788\right) r\,(1 + 0.000448 r)\right] \quad \text{(A4)}$$

Equivalent temperature, $T_E$, is $\theta_E$ scaled by $\pi$:

$$T_E = \theta_E \pi \quad \text{(A5)}$$

The initial guess for $T_w$ is based upon regions where the second order derivative of $\theta_E$ reaches a linear relationship with variations in $T_w$ and $\lambda$. Two coefficients are derived (Davies-Jones, 2008):

$$k1 = -38.5\pi^2 + 137.81\pi - 53.737 \quad \text{(A6)}$$

$$k2 = -4.392\pi^2 + 56.831\pi - 0.384 \quad \text{(A7)}$$

The initial guess of $T_w$ for coldest temperatures:

$$T_w = T_E - C - \frac{A r_s(T_E,\pi)}{1 + A r_s(T_E,\pi)\frac{\partial \ln(e_s)}{\partial T_E}} \quad \text{(A8)}$$

where $C$ is freezing temperature, $A$ is a constant (2675), and $r_s$ is the saturated mixing ratio. The evaluation of errors at a various pressures necessitated that Davies-Jones develop a regression line on colder regions of the initial guess:

$$(C/T_E)^{\lambda} > D(\pi); \quad D = \left(0.1859\frac{p}{p_0} + 0.6512\right)^{-1} \quad \text{(A9)}$$





GMDD
7, 5197–5248, 2014

where $D$ is calculating transition points between quadratic fits to the second order derivatives of $\theta_E$. $T_w$ for all other temperature regimes is governed by:

$$T_w = k1(\pi) - 1.21\mathrm{cold} - 1.45\mathrm{hot} - (k2(\pi) - 1.21\mathrm{cold})\left(C/T_E\right)^\lambda + \left(\frac{0.58}{\left(C/T_E\right)^\lambda}\right)\mathrm{hot} \tag{A10}$$

$$\mathrm{cold}\begin{cases} = 0 : 1 \leq \left(C/T_E\right)^\lambda \leq D(\pi) \\ = 1 \end{cases} \tag{A11}$$

$$\mathrm{hot}\begin{cases} = 1 : T_E > 355.15 \\ = 0 \end{cases} \tag{A12}$$

where the combination of equations' initial guesses are valid from 1050 mb down to 100 mb. Following the initial guess, up to two iterations using the Newton–Raphson method are required to reach the true wet bulb temperature. Using $T_W$, saturation vapor pressure is solved by the August–Roche–Magnus formulation of the Clausius–Clayperon equation (Bolton, 1980; Lawrence, 2005):

$$e_s(T_W) = 6.112\exp\left(\frac{a(T_W - C)}{T_W - C + b}\right) \tag{A13}$$

where $e_s$ is in mb, a and b are constants. The saturation mixing ratio, $r_s$, is dependent on $e_s$:

$$r_s(T_W) = \frac{\varepsilon e_s(T_W)}{\left(p_0\pi^\lambda - e_s(T_W)\right)} \tag{A14}$$

where $\varepsilon$ is a constant ($\sim 0.622$). Following Davies-Jones, we use the derivative of ARM equation for calculating the derivative of $r_s$:

$$\frac{\partial \ln(e_s)}{\partial T_W} = \frac{ab}{(T_W - C + b)^2} \tag{A15}$$

$$\frac{\partial e_s}{\partial T_W} = e_s \frac{\partial \ln(e_s)}{\partial T_W} \tag{A16}$$

$$\left(\frac{\partial r_s}{\partial T_W}\right)_\pi = \frac{\varepsilon p}{(p - e_s(T_W))^2} \frac{\partial e_s}{\partial T_W} \tag{A17}$$

Now, we return to $\theta_E$, and substitute $T_W$ for $T_L$:

$$f(T_W;\pi) = (C/T_W)^\lambda \left[1 - \frac{e_s}{p_0 \pi^\lambda}\right]^{\kappa_d \lambda} \exp(-\lambda G(T_W;\pi)) \tag{A18}$$

where:

$$G(T_W;\pi) = \left(\frac{3036}{T_W} - 1.78\right)\left[r_s(T_W;\pi) + 0.448 r_s^2(T_W;\pi)\right] \tag{A19}$$

The derivative of the function Eq. (A18) is required for the Newton–Raphson method:

$$f'(T_W;\pi) = -\lambda \left[\frac{1}{T_W} + \frac{\kappa_d}{(p - e_s(T_W))} \frac{\partial e_s}{\partial T_W} + \left(\frac{\partial G}{\partial T_W}\right)_\pi\right] \tag{A20}$$

where the derivative of $G(T_W;\pi)$:

$$\left(\frac{\partial G}{\partial T_W}\right)_\pi = -\frac{3036\left(r_s(T_W) + 0.448 r_s^2(T_W)\right)}{T_W^2} \left(\frac{3036}{T_W} - 1.78\right)$$
$$(1 + 2(0.448 r_s(T_W))) \left(\frac{\partial r_s}{\partial T_W}\right)_\pi \tag{A21}$$



GMDD
7, 5197–5248, 2014
Implementation and comparison of a suite of heat stress metrics
J. R. Buzan et al.

and, due to the linear relationship of the second order derivative of Eq. (A18), we may accelerate the Newton–Raphson method using the initially calculated $T_W$ and $T_E$:

$$T_w = T_w - \frac{f\left(T_W;\pi\right) - \left(C/T_E\right)^{\lambda}}{f'\left(T_W;\pi\right)} \tag{A22}$$

*Acknowledgements.* This research was supported by computing resources from Information Technology at Purdue University. JRB thanks Aaron Goldner, Jacob Carley, and Nick Herold for helpful comments and support. He also thanks his friends for their continued, unwavering, support. Finally, J. R. Buzan thanks his family. K. W. Oleson acknowledges support from the NCAR WCIASP and from NASA grant NNX10AK79G (the SIMMER project). NCAR is sponsored by the National Science Foundation.

## References

Adam-Poupart, A., LaBreche, F., Smargiassi, A., Duguay, P., Busque, M., Gagne, C., Rintamaki, H., Kjellstrom, T., and Zayed, J.: Climate change and occupational health and safety in a temperate climate: potential impacts and research priorities in Quebec, Canada, Ind. Health, 51, 68–78, 2013.

American College of Sports Medicine: Position stand on the prevention of thermal injuries during distance running, Med. J. Australia, 141, 876–879, 1984.

American College of Sports Medicine: Position stand on the prevention of thermal injuries during distance running, Med. Sci. Sport. Exer., 19, 529–533, 1987.

Alfano, F. R. D. A., Palella, B. I., and Riccio, G.: On the problems related to natural wet bulb temperature indirect evaluation for the assessment of hot thermal environments by means of WBGT, Ann. Occup. Hyg., 56, 1063–1079, 2012.

Australian Bureau of Meteorology: About the WBGT and Apparent Temperature Indices – Australian Bureau of Meteorology, available at: http://www.bom.gov.au/info/thermal_stress/ (last access: 16 March 2014), 2014.

Barriopedro, D., Fischer, E., Luterbacher, J., Trigo, R., and García-Herrera, R.: The hot summer of 2010: redrawing the temperature record map of Europe, Science, 332, 220–224, 2011.

Belding, H. S. and Hatch, T. F.: Index for evaluating heat stress in terms of resulting physiological strain, in: Heating, Piping and Air Conditioning, 27, 129 pp., 1955.

Benestad, R. E.: A new global set of downscaled temperature scenarios, J. Climate, 24, 2080–2098, 2011.

Berglund, L. G. and Yokota, M.: Comparison of Human Responses to Prototype and Standard Uniforms Using Three Different Human Simulation Models: HSDA, Scenario_J and Simulink2NM (No. USARIEM-T05-08), Army Research Inst of Environmental Medicine Natick MA Biophysics and Biomedical Modeling Div, 2005.

Betts, A. K. and Dugan, F. J.: Empirical formula for saturation pseudoadiabats and saturation equivalent potential temperature, J. Appl. Meteorol., 12, 731–732, 1973.

Bolton, D.: The computation of equivalent potential temperature, Mon. Weather Rev., 108, 1046–1053, 1980.

Bonan, G. B., Levis, S., Kergoat, L., and Oleson, K. W.: Landscapes as patches of plant functional types: an integrating concept for climate and ecosystem models, Global Biogeochem. Cy., 16, 1021, doi:10.1029/2000GB001360, 2002.

Brake, D. J.: Calculation of the natural (unventilated) wet bulb temperature, psychrometric dry bulb temperature and wet bulb globe temperature from standard psychrometric measurements, J. Mine Vent. Soc. S. Afr., 54, 108–112, 2001.

Breckenridge, J. R. and Goldman, R. F.: Solar heat load in man, J. Appl. Physiol., 31, 659–663, 1971.

Bröde, P., Krüger, E. L., Rossi, F. A., and Fiala, D.: Predicting urban outdoor thermal comfort by the Universal Thermal Climate Index UTCI – a case study in southern Brazil, Int. J. Biometeorol., 56, 471–480, 2012.

Bröde, P., Blazejczyk, K., Fiala, D., Havenith, G., Holmer, I., Jendritzky, G., Kuklane, K., and Kampmann, B.: The Universal Thermal Climate Index UTCI compared to ergonomics standards for assessing the thermal environment, Ind. Health, 51, 16–24, 2013.

Brooks, R. H. and Corey, T.: Hydraulic properties of porous media, Hydrology Papers, Colorado State University, Fort Colins, Colorado, 3, 1–30, 1964.

Budd, G. M.: Wet-Bulb Globe Temperature (WBGT) – its history and its limitations, J. Sci. Med. Sport, 11, 20–32, 2008.

Casado, M., Ortega, P., Masson-Delmotte, V., Risi, C., Swingedouw, D., Daux, V., Genty, D., Maignan, F., Solomina, O., Vinther, B., Viovy, N., and Yiou, P.: Impact of precipitation intermit-





GMDD
7, 5197–5248, 2014

tency on NAO-temperature signals in proxy records, Clim. Past, 9, 871–886, doi:10.5194/cp-9-871-2013, 2013.
Chan, A. P., Yam, M. C., Chung, J. W., and Yi, W.: Developing a heat stress model for construction workers, Journal of Facilities Management, 10, 59–74, 2012.
Cook, K. H., Meehl, G. A., and Arblaster, J. M.: Monsoon regimes and processes in CCSM4. Part II: African and American monsoon systems, J. Climate, 25, 2609–2621, 2012.
Davies-Jones, R.: An efficient and accurate method for computing the wet-bulb temperature along pseudoadiabats, Mon. Weather Rev., 136, 2764–2785, 2008.
Davies-Jones, R.: On formulas for equivalent potential temperature, Mon. Weather Rev., 137, 3137–3148, 2009.
Diffenbaugh, N. S., Pal, J. S., Giorgi, F., and Gao, X.: Heat stress intensification in the Mediterranean climate change hotspot, Geophys. Res. Lett., 34, L11706, doi:10.1029/2007GL030000, 2007.
Dufton, A. M.: The Eupatheostat, J. Sci. Instrum., 6, 249–251, 1929.
Dunne, J. P., Stouffer, R. J., and John, J. G.: Reductions in labour capacity from heat stress under climate warming, Nat. Clim. Change, 3, 563–566, doi:10.1038/nclimate1827, 2013.
Epstein, Y. and Moran, D. S.: Thermal comfort and the heat stress indices, Ind. Health, 44, 388–398, 2006.
Fiala, D., Lomas, K. J., and Stohrer, M.: A computer model of human thermoregulation for a wide range of environmental conditions: the passive system, J. Appl. Physiol., 87, 1957–1972, 1999.
Fiala, D., Lomas, K. J., and Stohrer, M.: Computer prediction of human thermoregulatory and temperature responses to a wide range of environmental conditions, Int. J. Biometeorol., 45, 143–159, 2001.
Fiala, D., Psikuta, A., Jendritzky, G., Paulke, S., Nelson, D., D. van Marken Lichtenbelt, W., and Frijns., W.: Physiological modeling for technical, clinical and research applications, Front Biosci. S., 2, 939–968, 2010.
Fiala, D., Havenith, G., Brode, P., Kampmann, B., and Jendritzky, G.: UTCI-Fiala multi-node model of human heat transfer and temperature regulation, Int. J. Biometeorol., 56, 429–441, doi:10.1007/s00484-011-0424-7, 2011.
Fischer, E. M. and Knutti, R.: Robust projections of combined humidity and temperature extremes, Nat. Clim. Change, 3, 126–130, doi:10.1038/nclimate1682, 2012.





GMDD
7, 5197–5248, 2014

Fischer, E. M. and Schar, C.: Consistent geographical patterns of changes in high-impact European heatwaves, Nat. Geosci., 3, 398–403, doi:10.1038/ngeo866, 2010.
Fischer, E. M., Seneviratne, S., Luthi, D., and Schar, C.: Contribution of land–atmosphere coupling to recent European summer heat waves, Geophys. Res. Lett., 34, L06707, doi:10.1029/2006GL029068, 2007.
Fischer, E. M., Oleson, K. W., and Lawrence, D. M.: Contrasting urban and rural heat stress responses to climate change, Geophys. Res. Lett., 39, L03705, doi:10.1029/2011GL050576, 2012.
Flatau, P. J., Walko, R. L., and Cotton, W. R.: Polynomial fits to saturation vapor pressure, J. Appl. Meteorol., 31, 1507–1507, 1992.
Gagge, A. P.: An effective temperature scale based on a simple model of human physiological regulatory response, ASHRAE Tran., 77, 247–262, 1972.
García-Herrera, R., Diaz, J., Trigo, R. M., Luterbacher, J., and Fischer, E. M.: A review of the European summer heat wave of 2003, Critical Reviews in Environmental Science and Technology, 40, 267–306, 2010.
Gates, R. S., Timmons, M. B., and Bottcher, R. W.: Numerical optimization of evaporative misting systems, T. ASAE, 34, 275–280, 1991a.
Gates, R. S., Usry, J. L., Nienaber, J. A., Turner, L. W., and Bridges, T. C.: An optimal misting method for cooling livestock housing, T. ASAE, 34, 2199–2206, doi:10.13031/2013.31859, 1991b.
Giles, B. D., Balafoutis, C., and Maheras, P.: Too hot for comfort: the heatwaves of Greece in 1987 and 1988, Int. J. Biometeorol., 34, 98–104, 1990.
Gonzalez, R. R.: SCENARIO revisited: comparisons of operational and rational models in predicting human responses to the environment, J. Therm. Biol., 29, 515–527, 2004.
Gonzalez, R. R., Cheuvront, S. N., Ely, B. R., Moran, D. S., Hadid, A., Endrusick, T. L., and Sawka, M. N.: Sweat rate prediction equations for outdoor exercise with transient solar radiation, J. Appl. Physiol., 112, 1300–1310, 2012.
Haslam, R. and Parsons, K.: Using computer-based models for predicting human thermal responses to hot and cold environments, TERG, 37, 399–416, 1994.
Havenith, G., Fiala, D., Błazejczyk, K., Richards, M., Bröde, P., Holmér, I., Rintamaki, H., Benshabat, Y., and Jendritzky, G.: The UTCI-clothing model, Int. J. Biometeorol., 56, 461–470, 2012.





GMDD
7, 5197–5248, 2014

Departments of the Army and Air Force: Heat Stress Control and Heat Casualty Management, Technical Bulletin Medical 507/Air Force Pamphlet, US Army, 48–152, 2003.
Höppe, P.: The physiological equivalent temperature – a universal index for the biometeorological assessment of the thermal environment, Int. J. Biometeorol., 43, 71–75, 1999.
Houghton, F. and Yaglou, C.: Determining equal comfort lines, J. Am. Soc. Heat. Vent. Eng., 29, 165–176, 1923.
Hurrell, J. W., Holland, M. M., Gent, P. R., Ghan, S., Kay, J. E., Kushner, P. J., Lamarque, J. F., Large, W. G., Lawrence, D., Lindsay, K., Lipscomb, W. H., Long, M. C., Mahowald, N., Marsh, D. R., Neale, R. B., Rasch, P., Vavrus, S., Vertenstein, M., Bader, D., Collins, W. D., Hack, J. J., Kiehl, J., and Marshall, S.: The Community Earth System Model: a framework for collaborative research, B. Am. Meteorol. Soc., 94, 1339–1360, doi:10.1175/bams-d-12-00121.1, 2013.
Hyatt, O. M., Lemke, B., and Kjellstrom, T.: Regional maps of occupational heat exposure: past, present, and potential future, Global Health Action, 3, 5715, doi:10.3402/gha.v3i0.5715, 2010.
Ingram, D. L.: Evaporative cooling in the pig, Nature, 207, 415–416, 1965.
Jendritzky, G. and Tinz, B.: The thermal environment of the human being on the global scale, Global Health Action, 2, 2005, doi:10.3402/gha.v2i0.2005, 2009.
Jendritzky, G., Havenith, G., Weihs, P., and Batchvarova, E.: Towards a Universal Thermal Climate Index UTCI for assessing the thermal environment of the human being, Final Report COST Action, 730, 1–26, 2009.
Kalnay, E., Kanamitsu, M., Kistler, R., Collins, W., Deaven, D., Gandin, L., Iredell, M., Saha, S., White, G., Woollen, J., Zhu, Y., Chelliah, M., Ebisuzaki, W., Higgins, W., Janowiak, J., Mo, K. C., Ropelewski, C., Wang, J., Leetmaa, A., Reynolds, R., Jenne, R., and Joseph, D.: The NCEP/NCAR 40-year Reanalysis Project, B. Am. Meteorol. Soc., 77, 437–471, 1996.
Khan, Z. A., Maniyan, S., Mokhtar, M., Quadir, G. A., and Seetharamu, K. N.: A generalised transient thermal model for human body, Jurnal Mekanikal, 18, 78–97, 2004.
Kjellstrom, T., Gabrysch, S., Lemke, B., and Dear, K.: The “Hothaps” programme for assessing climate change impacts on occupational health and productivity: an invitation to carry out field studies, Global Health Action, 2, 2082, doi:10.3402/gha.v2i0.2082, 2009a.
Kjellstrom, T., Kovats, R. S., Lloyd, S. J., Holt, T., and Tol, R. S.: The direct impact of climate change on regional labor productivity, Arch. Environ. Occup. H., 64, 217–227, 2009b.

Kjellstrom, T., Holmer, I., and Lemke, B.: Workplace heat stress, health and productivity – an increasing challenge for low and middle-income countries during climate change, Global Health Action, 2, 2047, doi:10.3402/gha.v2i0.2047, 2009c.

Kjellstrom, T., Lemke, B., and Otto, M.: Mapping occupational heat exposure and effects in South-East Asia: ongoing time trends 1980–2011 and future estimates to 2050, Ind. Health, 51, 56–67, 2013.

Koca, R. W., Hughes, W. C., and Christianson, L. L.: Evaporative cooling pads: test procedure and evaluation, Appl. Eng. Agric., 7, 485–490, 1991.

Kraning, K. K. and Gonzalez, R. R.: A mechanistic computer simulation of human work in heat that accounts for physical and physiological effects of clothing, aerobic fitness, and progressive dehydration, J. Therm. Biol., 22, 331–342, 1997.

Keuhn, L. A., Stubbs, R. A., and Weaver, R. S.: Theory of the Globe Thermometer (No. DRET-RP-745), Defense Research Establishment Toronto Downsview, Ontario, 1970.

Lawrence, D. M., Oleson, K. W., Flanner, M. G., Thornton, P. E., Swenson, S. C., Lawrence, P. J., Zeng, X., Yang, Z.-L., Levis, S., Sakaguchi, K., Bonan, G. B., and Slater, A. G.: Parameterization improvements and functional and structural advances in version 4 of the Community Land Model, J. Adv. Model. Earth Syst., 3, M03001, doi:10.1029/2011MS000045, 2011.

Lawrence, M. G.: The relationship between relative humidity and the dewpoint temperature in moist air: a simple conversion and applications, B. Am. Meteorol. Soc., 86, 225–233, 2005.

Liang, C., Zheng, G., Zhu, N., Tian, Z., Lu, S., and Chen, Y.: A new environmental heat stress index for indoor hot and humid environments based on Cox regression, Build. Environ., 46, 2472–2479, 2011.

Liljegren, J. C., Carhart, R. A., Lawday, P., Tschopp, S., and Sharp, R.: Modeling the wet bulb globe temperature using standard meteorological measurements, J. Occup. Environ. Hyg., 5, 645–655, 2008.

Lucas, E. M., Randall, J. M., and Meneses, J. F.: Potential for evaporative cooling during heat stress periods in pig production in Portugal (Alentejo), J. Agr. Eng. Res., 76, 363–371, 2000.

Maloney, S. K. and Forbes, C. F.: What effect will a few degrees of climate change have on human heat balance? Implications for human activity, Int. J. Biometeorol., 55, 147–160, 2011.

Masterson, J. M. and Richardson, F. A.: Humidex, a method of quantifying human discomfort due to excessive heat and humidity, Environment Canada, Atmospheric Environment Service, Downsview, Ontario, CLI 1–79, 1979.





GMDD
7, 5197–5248, 2014

Implementation and comparison of a suite of heat stress metrics

J. R. Buzan et al.

Meehl, G. A. and Tebaldi, C.: More intense, more frequent, and longer lasting heat waves in the 21st century, Science, 305, 994–7, 2004.
Meehl, G. A., Arblaster, J. M., Lawrence, D. M., Seth, A., Schneider, E. K., Kirtman, B. P., and Min, D.: Monsoon regimes in the CCSM3, J. Climate, 19, 2482–2495, 2006.
Minard, D., Belding, H. S., and Kingston, J. R.: Prevention of heat casualties, J. Amer. Med. Assoc., 165, 1813–1818, 1957.
Miralles, D., Teuling, A., Van Heerwaarden, C., and Arellano, J.: Mega-heatwave temperatures due to combined soil desiccation and atmospheric heat accumulation, Nat. Geosci., 7, 345–349, 2014.
Mitchell, T. D. and Jones, P. D.: An improved method of constructing a database of monthly climate observations and associated high-resolution grids, Int. J. Climatol., 25, 693–712, 2005.
Moran, D. S., Pandolf, K. B., Shapiro, Y., Heled, Y., Shani, Y., Mathew, W. T., and Gonzalez, R. R.: An environmental stress index (ESI) as a substitute for the wet bulb globe temperature (WBGT), J. Therm. Biol., 26, 427–431, 2001.
Mueller, B. and Seneviratne, S.: Hot days induced by precipitation deficits at the global scale, P. Natl. Acad. Sci. USA, 109, 12398–12403, 2012.
Nag, P., Dutta, P., and Nag, A.: Critical body temperature profile as indicator of heat stress vulnerability, Ind. Health, 51, 113–122, 2013.
Nilsson, M. and Kjellstrom, T.: Climate change impacts on working people: how to develop prevention policies, Global Health Action, 3, 5774, doi:10.3402/gha.v3i0.5774, 2010.
NOAAWatch: Heat Wave: A Major Summer Killer, available at: http://www.noaawatch.gov/themes/heat.php (last access: 12 March 2014), 2014.
Oke, T. R.: Boundary Layer Climates, 2nd edn., Methuen and Co., London, Chapter 4, 124–127, 1987.
Oleson, K.: Contrasts between urban and rural climate in CCSM4 CMIP5 climate change scenarios, J. Climate, 25, 1390–1412, 2012.
Oleson, K. W., Niu, G. Y., Yang, Z. L., Lawrence, D. M., Thornton, P. E., Lawrence, P. J., Stockli, R., Dickinson, R. E., Bonan, G. B., Levis, S., Dai, A., and Qian, T.: Improvements to the Community Land Model and their impact on the hydrological cycle, J. Geophys. Res.-Biogeo., 113, G01021, doi:10.1029/2007JG000563, 2008a.

Oleson, K. W., Bonan, G. B., Feddema, J., Vertenstein, M., and Grimmond, C. S. B.: An urban parameterization for a global climate model, Part I: Formulation and evaluation for two cities, J. Appl. Meteorol. Clim., 47, 1038–1060, 2008b.
Oleson, K. W., Bonan, G. B., Feddema, J., and Vertenstein, M.: An urban parameterization for a global climate model, Part II: Sensitivity to input parameters and the simulated urban heat island in offline simulations. J. Appl. Meteorol. Clim., 47, 1061–1076, 2008c.
Oleson, K. W., Lawrence, D. M., Bonan, G. B., Flanner, M. G., Kluzek, E., Lawrence, P. J., Levis, S., Swenson, S. C., Thornton, P. E., Dai, A., Decker, M., Dickinson, R., Feddema, J., Heald, C. L., Hoffman, F., Lamarque, J.-F., Mahowald, N., Niu, G.-Y., Qian, T., Randerson, J., Running, S., Sakaguchi, K., Slater, A., Stockli, R., Wang, A., Yang, Z.-L., Zeng, X., and Zeng, X.: Technical Description of version 4.0 of the Community Land Model (CLM), NCAR Technical Note NCAR/TN-478+STR, National Center for Atmospheric Research, Boulder, CO, 257 pp., 2010a.
Oleson, K. W., Bonan, G. B., Feddema, J., Vertenstein, M., and Kluzek, E.: Technical Description of an Urban Parameterization for the Community Land Model (CLMU), NCAR Technical Note NCAR/TN-480+STR, doi:10.5065/D6K35RM9, 2010b.
Oleson, K. W., Bonan, G. B., Feddema, J., and Jackson, T.: An examination of urban heat island characteristics in a global climate model, Int. J. Climatol., 31, 1848–1865, 2011.
Oleson, K. W., Lawrence, D. M., Bonan, G. B., Drewniak, B., Huang, M., Koven, C. D., Levis, S., Li, F., Riley, W. J., Subin, Z. M., Swenson, S. C., Thornton, P. E., Bozbiyik, A., Fisher, R., Kluzek, E., Lamarque, J.-F., Lawrence, P. J., Leung, L. R., Lipscomb, W., Muszala, S., Ricciuto, D. M., Sacks, W., Sun, Y., Tang, J., and Yang, Z.-L.: Technical Description of version 4.5 of the Community Land Model (CLM), NCAR Technical Note NCAR/TN-503+STR, National Center for Atmospheric Research, Boulder, CO, 422 pp., doi:10.5065/D6RR1W7M, 2013a.
Oleson, K. W., Monaghan, A., Wilhelmi, O., Barlage, M., Brunsell, N., Feddema, J., Hu, L., and Steinhoff, D. F.: Interactions between urbanization, heat stress, and climate change, Climatic Change, 1–17, doi:10.1007/s10584-013-0936-8, 2013b.
Parsons, K.: Heat stress standard ISO 7243 and its global application, Ind. Health, 44, 368–379, 2006.
Parsons, K.: Occupational health impacts of climate change: current and future ISO standards for the assessment of heat stress, Ind. Health, 51, 86–100, 2013.





GMDD
7, 5197–5248, 2014

Pradhan, B., Shrestha, S., Shrestha, R., Pradhanang, S., Kayastha, B., and Pradhan, P.: Assessing climate change and heat stress responses in the Tarai region of Nepal, Ind. Health, 51, 101–12, 2013.

Renaudeau, D., Collin, A., Yahav, S., De Basilio, V., Gourdine, J. L., and Collier, R. J.: Adaptation to hot climate and strategies to alleviate heat stress in livestock production, Animal, 6, 707–728, 2012.

Rothfusz, L. P. and Headquarters, N. S. R.: The heat index equation (or, more than you ever wanted to know about heat index), Fort Worth, Texas: National Oceanic and Atmospheric Administration, National Weather Service, Office of Meteorology, 90–23, 1990.

Scholander, P., Hock, R., Walters, V., and Irving, L.: Adaptation to cold in arctic and tropical mammals and birds in relation to body temperature, insulation, and basal metabolic rate, Biol. Bull., 99, 259–271, 1950.

Seneviratne, S. I., Nicholls, N., Easterling, D., Goodess, C. M., Kanae, S., Kossin, J., Luo, Y., Marengo, J., McInnes, K., Rahimi, M., Reichstein, M., Sorteberg, A., Vera, C., and Zhang, X.: Changes in climate extremes and their impacts on the natural physical environment, in: Managing the Risks of Extreme Events and Disasters to Advance Climate Change Adaptation, edited by: Field, C. B., Barros, V., Stocker, T. F., Qin, D., Dokken, D. J., Ebi, K. L., Mastrandrea, M. D., Mach, K. J., Plattner, G.-K., Allen, S. K., Tignor, M., and Midgley, P. M., A Special Report of Working Groups I and II of the Intergovernmental Panel on Climate Change (IPCC), Cambridge University Press, Cambridge, UK, and New York, NY, USA, 109–230, 2012.

Seneviratne, S., Donat, M., Mueller, B., and Alexander, L.: No pause in the increase of hot temperature extremes, Nat. Clim. Change, 4, 161–163, 2014.

Sheffield, P. E., Herrera, J. G. R., Lemke, B., Kjellstrom, T., and Romero, L. E. B.: Current and future heat stress in nicaraguan work places under a changing climate, Ind. Health, 51, 123–127, 2013.

Sherwood, S. C. and Huber, M.: An adaptability limit to climate change due to heat stress, P. Natl. Acad. Sci. USA, 107, 9552–9555, 2010.

Simpson, R. H.: On the computation of equivalent potential temperature, Mon. Weather Rev., 106, 124–130, 1978.

Smith, R. K. and Montgomery, M. T.: How important is the isothermal expansion effect in elevating equivalent potential temperature in the hurricane inner core?, Q. J. Roy. Meteor. Soc., 139, 70–74, doi:10.1002/qj.1969, 2012.





GMDD
7, 5197–5248, 2014

SREX IPCC: Summary for policymakers, in: Managing the Risks of Extreme Events and Disasters to Advance Climate Change Adaptation, edited by: Field, C. B., Barros, V., Stocker, T. F., Qin, D., Dokken, D. J., Ebi, K. L., Mastrandrea, M. D., Mach, K. J., Plattner, G.-K., Allen, S. K., Tignor, M., and Midgley, P. M., A Special Report of Working Groups I and II of the Intergovernmental Panel on Climate Change, Cambridge University Press, Cambridge, UK, and New York, NY, USA, 1–19, 2012.

Steadman, R. G.: The assessment of sultriness, Part I: A temperature-humidity index based on human physiology and clothing science, J. Appl. Meteorol., 18, 861–873, 1979a.

Steadman, R. G.: The assessment of sultriness, Part II: Effects of wind, extra radiation and barometric pressure on apparent temperature, J. Appl. Meteorol., 18, 874–884, 1979b.

Steadman, R. G.: A universal scale of apparent temperature, J. Clim. Appl. Meteorol., 23, 1674–1687, 1984.

Steadman, R. G.: Norms of apparent temperature in Australia, Aust. Met. Mag., 43, 1–16, 1994.

Stoecklin-Marois, M., Hennessy-Burt, T., Mitchell, D., and Schenker, M.: Heat-related illness knowledge and practices among California hired farm workers in the MICASA study, Ind. Health, 51, 47–55, 2013.

Stolwijk, J.: A Mathematical Model of Physiological Temperature Regulation in Man, Report CR-1855 NASA, Washington, DC, 1971.

Stolwijk, J.: Mathematical models of thermal regulation, Ann. NY Acad. Sci., 335, 98–106, 1980.

Stolwijk, J. and Hardy, J.: Temperature regulation in man – a theoretical study, Ptlilgers Archiv, 129, 129–162, 1966.

Stull, R.: Wet-bulb temperature from relative humidity and air temperature, J. Appl. Meteorol. Clim., 50, 2267–2269, 2011.

Tawatsupa, B., Yiengrugsawan, V., Kjellstrom, T., Berecki-Gisolf, J., Seubsman, S., and Sleigh, A.: Association between heat stress and occupational injury among Thai workers: findings of the Thai Cohort Study, Ind. Health, 51, 34–46, 2013.

Taylor, K. E., Stouffer, R. J., and Meehl, G. A.: An overview of CMIP5 and the experiment design, B. Am. Meteorol. Soc., 93, 485–498, 2012.

Thom, E. C.: The discomfort index, Weatherwise, 12, 57–61, 1959.

van Genuchten, M.: A closed-form equation for predicting the hydraulic conductivity of unsaturated soils, Soil Sci. Soc. Am. J., 44, 892–898, 1980.

Wexler, A.: Vapor pressure formulation for water in range 0 to 100 Degrees C, a revision, J. Res. NBS A Phys. Ch., 80, 775–785, 1976.
Wexler, A.: Vapor pressure formulation for ice, J. Res. NBS A Phys. Ch., 81, 5–19, 1977.
Willett, K. M. and Sherwood, S.: Exceedance of heat index thresholds for 15 regions under a warming climate using the wet-bulb globe temperature, Int. J. Climatol., 32, 161–177, 2012.
Wyndham, C. and Atkins, A.: A physiological scheme and mathematical model of temperature regulation in man, Pflügers Archiv, 303, 14–30, 1968.
Yokota, M., Berglund, L., Cheuvront, S., Santee, W., Latzka, W., Montain, S., Kolka, M., and Moran, D.: Thermoregulatory model to predict physiological status from ambient environment and heart rate, Comput. Biol. Med., 38, 1187–1193, 2008.
Zhang, D. L., Liu, Y., and Yau, M. K.: A multiscale numerical study of Hurricane Andrew (1992), Part V: Inner-core thermodynamics, Mon. Weather Rev., 130, 2745–2763, 2002.





GMDD
7, 5197–5248, 2014
Implementation and comparison of a suite of heat stress metrics
J. R. Buzan et al.

**Table 1.** Heat stress diagnostics and prognostic models.

| Metric | Type | Ref. |
|---|---|---|
| Wet Bulb Temperature | Temperature | Haldane (1905) |
| Effective Temperature | Index | Houghton and Yaglou (1923) |
| Equivalent Temperature | Temperature | Dufton (1929) |
| Heat Stress Index | Index | Belding and Hatch (1955) |
| Wet Bulb Globe Temperature | Index | Yaglou and Minard (1957) |
| Discomfort Index | Index | Thom (1959) |
| Temperature Humidity Index | Index | Ingram (1965) |
| Temp. Regulation in Man | Prognostic | Stolwijk and Hardy (1966) |
| Physiological Mathematical Model | Prognostic | Wyndham and Atkins (1968) |
| Solar Heat in Man | Index | Breckenridge and Goldman (1971) |
| Mathematical Model Temperature in Man | Prognostic | Stolwijk (1971) |
| New Effective Temperature | Index | Gagge (1972) |
| Humidex | Index | Masterson and Richardson (1979) |
| Sultriness Index | Index | Steadman (1979a) |
| Mathematical Model Thermal Regulation | Prognostic | Stolwijk (1980) |
| Apparent Temperature | Index | Steadman (1984) |
| Heat Index | Index | Rothfusz (1990) |
| Computer Based Thermal Response | Prognostic | Haslam and Parsons (1994) |
| SCENARIO | Prognostic | Kraning and Gonzalez (1997) |
| Computer Model Human Thermo-Regulation | Prognostic | Fiala et al. (1999, 2001) |
| PET | Index | Höppe (1999) |
| Environmental Stress Index | Index | Moran et al. (2001) |
| SCENARIO Monte Carlo | Prognostic | Gonzalez (2004) |
| Generalized Transient Thermal Model | Prognostic | Khan et al. (2004) |
| ISO 7243 WBGT | Index | Parsons (2006) |
| IDCA | Prognostic | Yokota et al. (2008) |
| Physiological Equivalent Temperature | Index | Jendritzky and Tinz (2009) |
| UTCI | Index | Fiala et al. (2010) |
| UTCI-Fiala Model | Index-Prognostic | Fiala et al. (2011) |
| Index of Equivalent Temperature | Index | Liang et al. (2011) |





GMDD
7, 5197–5248, 2014

**Table 2.** Moist temperature variables and heat stress metrics.

| Metric | Variable | Equation # | Output | Calculated |
|---|---|---|---|---|
| Temperature (Kelvin) | $T$ | N/A | X | X |
| Temperature (Celsius) | $T_c$ | N/A | | X |
| Pressure | $P$ | N/A | X | X |
| Relative humidity | RH | N/A | X | X |
| Specific humidity | $Q$ | N/A | X | X |
| 10 m Winds | $u_{10m}$ | N/A | X | X |
| Vapor Pressure | $e_{RH}$ | 2 | | X |
| Saturated vapor pressure | $e_s$ | A13 | | X |
| Derivative saturated vapor pressure | $de_s/dT$ | A16 | | X |
| Log derivative saturated vapor pressure | $d(\ln(e_s))/dT$ | A15 | | X |
| Mixing ratio | $r_s$ | A14 | | X |
| Derivative mixing ratio | $dr_s/dT$ | A17 | | X |
| Function of equivalent potential temperature | $f(\theta_E)$ | A18 | | X |
| Derivative of function of equivalent potential temperature | $f'(\theta_E)$ | A20 | | X |
| Wet Bulb Temperature | $T_w$ | A22 | X | X |
| Wet Bulb Temperature, Stull | $T_{wS}$ | 11–12 | X | X |
| Lifting condensation temperature | $T_L$ | A2 | | X |
| Moist potential temperature | $\theta_{DL}$ | A3 | | X |
| Equivalent potential temperature | $\theta_E$ | A4 | X | X |
| Equivalent temperature | $T_E$ | A5 | X | X |
| Heat Index | HI | 3 | X | X |
| Apparent Temperature | AT | 1 | X | X |
| Humidex | HUMIDEX | 4 | X | X |
| Wet Bulb Globe Temperature | WBGT | 8 | | |
| Indoor WBGT | indoorWBGT | 9 | | |
| Simplified WBGT | sWBGT | 10 | X | X |
| Universal Thermal Climate Index | UTCI | N/A | | |
| Discomfort Index | DI | 13 | X | X |
| Temperature Humidity Index | THI | 7 | | |
| Temperature Humidity Index for Comfort | THIC | 5 | X | X |
| Temperature Humidity Index for Physiology | THIP | 6 | X | X |
| Swamp cooler efficiency 65 % | SWMP65 | 15 | X | X |
| Swamp cooler efficiency 80 % | SWMP80 | 15 | X | X |





GMDD
7, 5197–5248, 2014

**Table 3.** Heat stress studies, modern and future.

| Location | Metric | Time | Model | Ref. |
|---|---|---|---|---|
| Mediterranean Sea | HI | Modern and Future | RegCM3 | Diffenbaugh et al. (2007) |
| Delhi | WBGT | Modern | NOAA | Kjellstrom et al. (2009a) |
| World | sWBGT | Future | HadCM3 | Kjellstrom et al. (2009b) |
| World Cities | WBGT, $T$ | Modern and Future | NOAA/Various Models | Kjellstrom et al. (2009c) |
| Global | PET variation | Future | ECHAM4 | Jendritzky and Tinz (2009) |
| Global | $T_w$ | Future | CCSM3 | Sherwood and Huber (2010) |
| Europe | HI, HUMIDEX | Future | ENSEMBLES | Fischer and Schar (2010) |
| Global | indoorWBGT | Modern and Future | NOAA | Hyatt et al. (2010) |
| Global | – | Modern | Assessment | Nilsson and Kjellstrom (2010) |
| Southern Brazil | UTCI | Modern | Direct Measurement | Bröde et al. (2012) |
| Global | sWBGT | Modern and Future | CLM4 | Fischer et al. (2012) |
| Global | sWBGT | Modern and Future | HadCRUH/ISD-NCDC | Willett and Sherwood (2012) |
| Global | $T$ | Modern | Various Datasets | SREX IPCC (2012) |
| Western India | WBGT, $T$ | Modern | Direct Measurement | Nag et al. (2013) |
| California Farms | – | Modern | Assessment | Stoecklin-Marois et al. (2013) |
| Thailand | – | Modern | Assessment | Tawatsupa et al. (2013) |
| Nepal | sWBGT, HI, HUMIDEX | Modern | Direct Measurement | Pradhan et al. (2013) |
| South East Asia | WBGT | Modern and Future | GSOD/CRU/BCM2 | Kjellstrom et al. (2013) |
| Quebec | $T$ | Future | Assessment | Adam-Poupart et al. (2013) |
| Global | indoorWBGT | Modern and Future | ESM2M/NCEP-NCAR | Dunne et al. (2013) |
| United States | sWBGT, DI, HI, HUMIDEX, AT | Modern and Future | CLM4/CLMU/WRF | Oleson et al. (2013b) |





GMDD
7, 5197–5248, 2014

**Table 4.** The HumanIndexMod: subroutine names, required inputs, and variables calculated.

| Name | Subroutine | Input | Calculates |
|---|---|---|---|
| Moist Thermodynamics | Wet_Bulb | $T$, $e_{RH}$, $P$, RH, $Q$ | $T_E$, $\theta_E$, $T_w$ |
| Wet Bulb Temperature, Stull | Wet_BulbS | $T_c$, RH | $T_{wS}$ |
| Heat Index | HeatIndex | $T_c$, RH | HI |
| Apparent Temperature | AppTemp | $T_c$, $e_{RH}$, $u_{10m}$ | AT |
| Simplified WBGT | swbgt | $T_c$, $e_{RH}$ | sWBGT |
| Humidex | hmdex | $T_c$, $e_{RH}$ | HUMIDEX |
| Discomfort Index | dis_coi | $T_c$, $T_w$ | DI |
| Discomfort Index w/Stull | dis_coiS | $T_c$, $T_{wS}$ | DI |
| Temperature Humidity Index | THIndex | $T_c$, $T_w$ | THIC, THIP |
| Swamp Cooler Efficiency | SwampCoolEff | $T_c$, $T_w$ | SWMP65, SWMP80 |
| Kelvin to Celsius | KtoC | $T$ | $T_c$ |
| Vapor Pressure | VaporPres | RH, $e_s$ | $e_{RH}$ |
| Saturated Vapor Pressure | QSat_2 | $T$, $P$ | $e_s$, $de_s/dT$, $d(\ln(e_s))/dT$, $r_s$, $dr_s/dT$, $f(\theta_E)$, $f'(\theta_E)$ |





GMDD
7, 5197–5248, 2014

**Table 5.** Regional city location and regime.

| City | Lat | Lon | Regime | City | Lat | Lon | Regime |
|---|---|---|---|---|---|---|---|
| Chicago | 41.52 | −87.37 | Mid-Latitude | Melbourne | −37.48 | 144.58 | Mid-Latitude |
| Paris | 48.51 | 2.21 | Mid-Latitude | Caracas | 10.29 | −66.54 | Equatorial |
| Moscow | 55.45 | 37.37 | Mid-Latitude | Bangkok | 13.43 | 100.28 | Convective |
| Beijing | 39.54 | 116.24 | Mid-Latitude | Monrovia | 6.18 | −10.47 | Equatorial |
| Singapore | 1.21 | 103.49 | Equatorial | Washington DC | 38.53 | −77.02 | Mid-Latitude |
| New Delhi | 28.37 | 77.13 | Convective | New Orleans | 29.57 | −90.04 | Convective |
| Islamabad | 33.43 | 73.03 | Convective | Miami | 25.47 | −80.63 | Convective |
| Cairo | 30.02 | 31.14 | Arid | Houston | 29.45 | −95.22 | Convective |
| Dodoma | −7.05 | 38.02 | Equatorial | San Francisco | 37.46 | −122.25 | Mid-Latitude |
| Darwin | −12.27 | 130.50 | Convective | Tel Aviv | 32.03 | 34.46 | Arid |
| Christchurch | −43.31 | 172.38 | Mid-Latitude | Port Said | 31.15 | 32.18 | Arid |
| Mexico City | 19.25 | −99.07 | Arid | Amman | 31.57 | 35.56 | Arid |
| Rio de Janeiro | −22.54 | −43.12 | Mid-Latitude | Beirut | 33.53 | 35.29 | Arid |
| Tokyo | 35.41 | 139.41 | Mid-Latitude | Damascus | 33.30 | 36.18 | Arid |
| La Paz | −16.29 | −68.08 | Arid | Aleppo | 36.12 | 37.09 | Arid |
| Jerusalem | 31.46 | 35.12 | Arid | Riyadh | 24.42 | 46.43 | Arid |
| Rome | 41.54 | 12.27 | Mid-Latitude | Mecca | 21.25 | 39.49 | Arid |
| Shanghai | 31.13 | 121.28 | Convective | Khamis Mushait | 18.18 | 42.44 | Arid |
| Chibi | 29.43 | 113.54 | Convective | Medina | 24.27 | 39.37 | Arid |
| Dhaka | 23.42 | 90.24 | Convective | Buraydah | 26.20 | 43.58 | Arid |
| Libreville | 0.20 | 9.22 | Equatorial | Dammam | 26.23 | 49.58 | Arid |





GMDD
7, 5197–5248, 2014

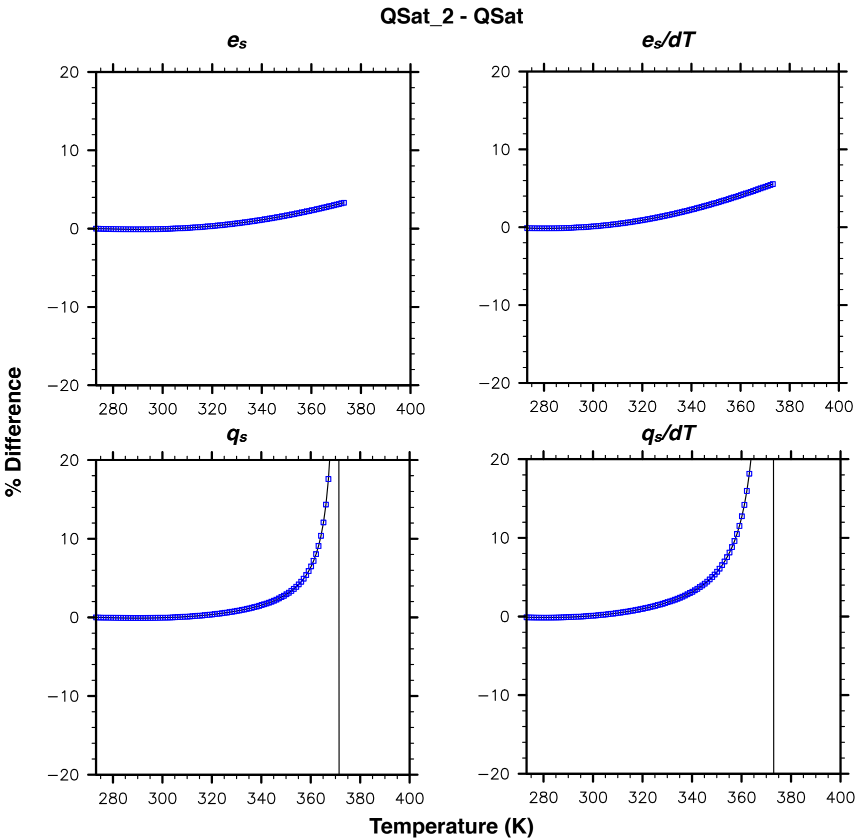


**Figure 1.** Differences between the QSat_2 and QSatMod algorithms at 1000 mb. Temperature along the $x$ axis and percent difference along the $y$ axis. Lower pressures show similar results (not shown). $q_s$ in both QSatMod and QSat_2 approach an asymptote when $e_s$ approaches $p$ in Eq. (A14). In QSat_2 $e_s$ approaches $p$ at slightly lower temperatures than QSatMod, and reaches the discontinuity first.

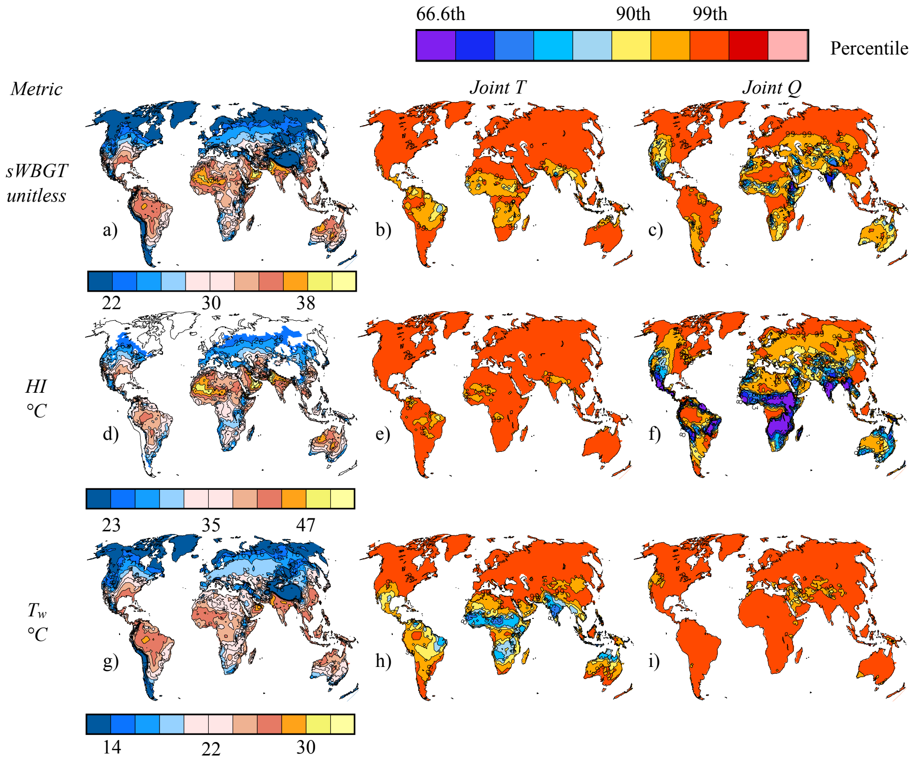


**Figure 2.** Joint distribution maps of the 99th percentile from 1901–2010 CLM4.5 forced by CRUNCEP. **(a)** sWBGT, **(b)** T_g_sWBGT, **(c)** Q_g_sWBGT, **(d)** HI, **(e)** T_g_HI, **(f)** Q_g_HI, **(g)** $T_w$, **(h)** T_g_$T_w$, **(i)** Q_g_$T_w$. **(a)**, **(d)**, and **(g)** are magnitude and use the color bar underneath their respective plot. **(b, c, e, f, h)**, and **(i)** use the percentile color bar. The joint distributions show the median percentile of the climatology that derived **(a, d)**, and **(g)**.





GMDD
7, 5197–5248, 2014

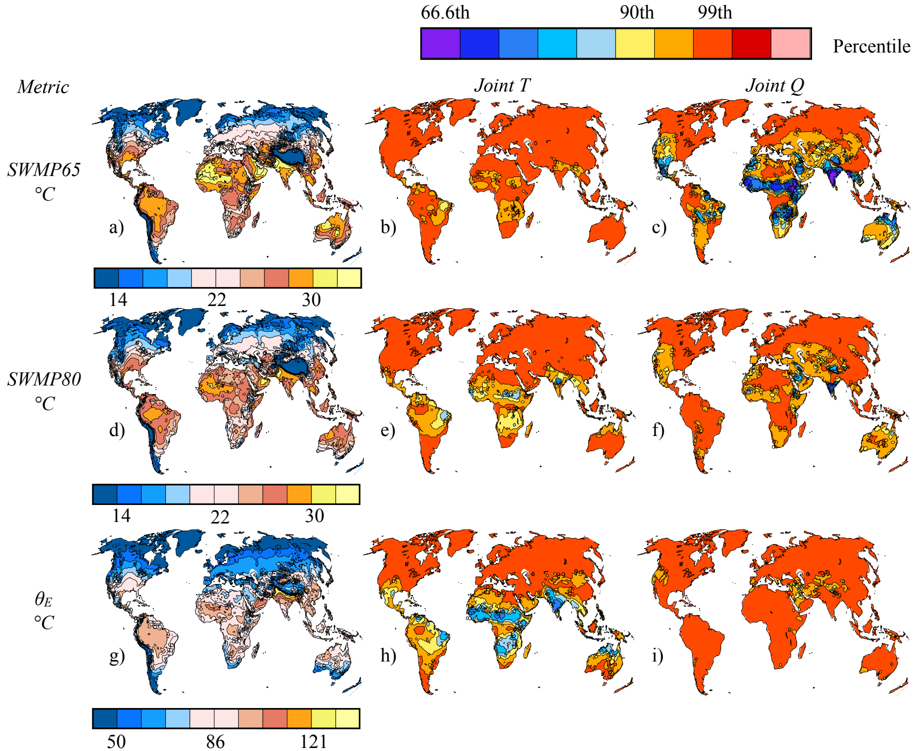


**Figure 3.** Description is same as in Fig. 2. **(a)** SWMP65, **(b)** T_g_SWMP65, **(c)** Q_g_SWMP65, **(d)** SWMP80, **(e)** T_g_SWMP80, **(f)** Q_g_SWMP80, **(g)** $\theta_E$, **(h)** T_g_$\theta_E$, **(i)** Q_g_$\theta_E$.





GMDD
7, 5197–5248, 2014

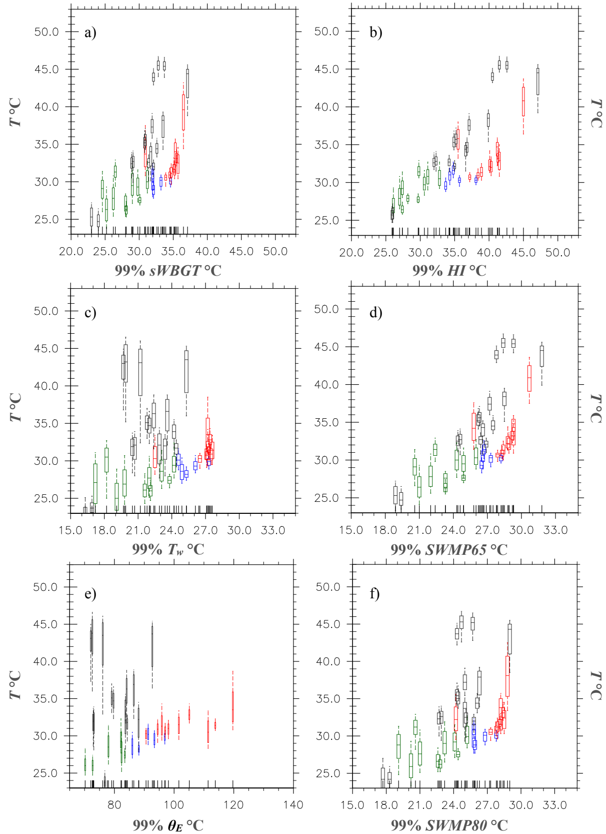


**Figure 4.** 1901–2010 CLM4.5 forced by CRUNCEP regional joint distribution box plots of $T$ magnitude from the 99th percentile. **(a)** T_g_sWBGT, **(b)** T_g_HI, **(c)** T_g_$T_w$, **(d)** T_g_SWMP65, **(e)** T_g_$\theta_E$, **(f)** T_g_SWMP80. Colors represent similar regional associations: convective (red), equatorial (blue), arid (grey), and mid-latitude (green).





GMDD
7, 5197–5248, 2014

Implementation and comparison of a suite of heat stress metrics

J. R. Buzan et al.

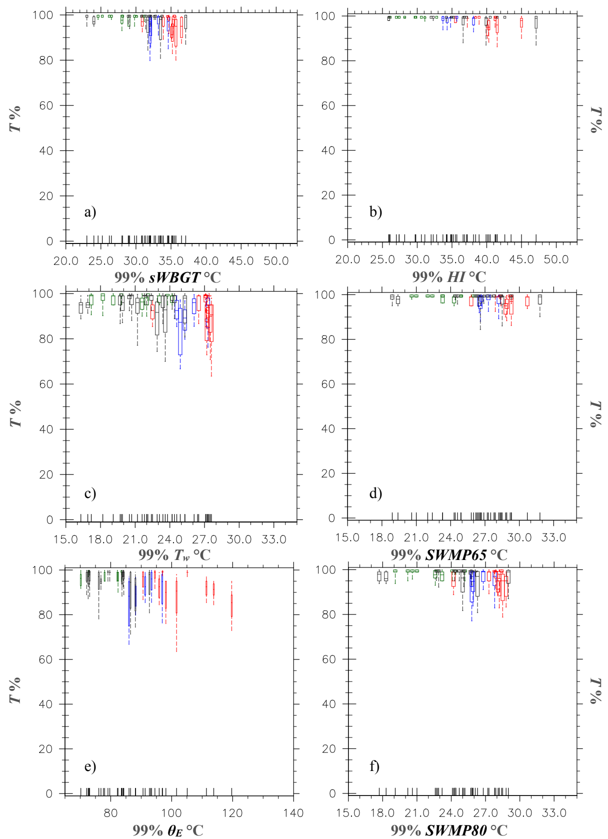


**Figure 5.** 1901–2010 CLM4.5 forced by CRUNCEP regional joint distribution box plots of $T$ climatological percent from the 99th percentile. **(a)** T_g_sWBGT, **(b)** T_g_HI, **(c)** T_g_$T_w$, **(d)** T_g_SWMP65, **(e)** T_g_$\theta_E$, **(f)** T_g_SWMP80. Colors are same as in Fig. 4.

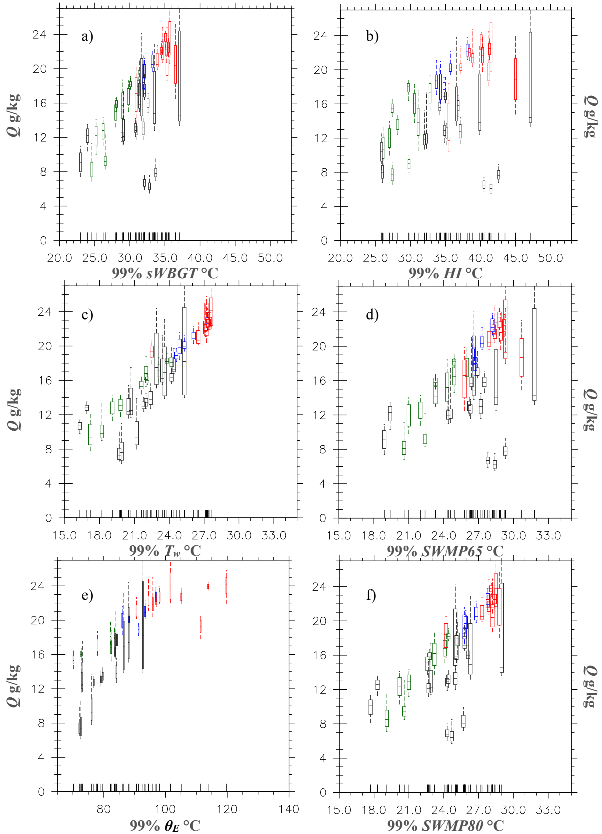


**Figure 6.** 1901–2010 CLM4.5 forced by CRUNCEP regional joint distribution box plots of $Q$ magnitude from the 99th percentile. **(a)** Q_g_sWBGT, **(b)** Q_g_HI, **(c)** Q_g_$T_w$, **(d)** Q_g_SWMP65, **(e)** Q_g_$\theta_E$, **(f)** Q_g_SWMP80. Colors are same as in Fig. 4.



GMDD

7, 5197–5248, 2014

Implementation and comparison of a suite of heat stress metrics

J. R. Buzan et al.

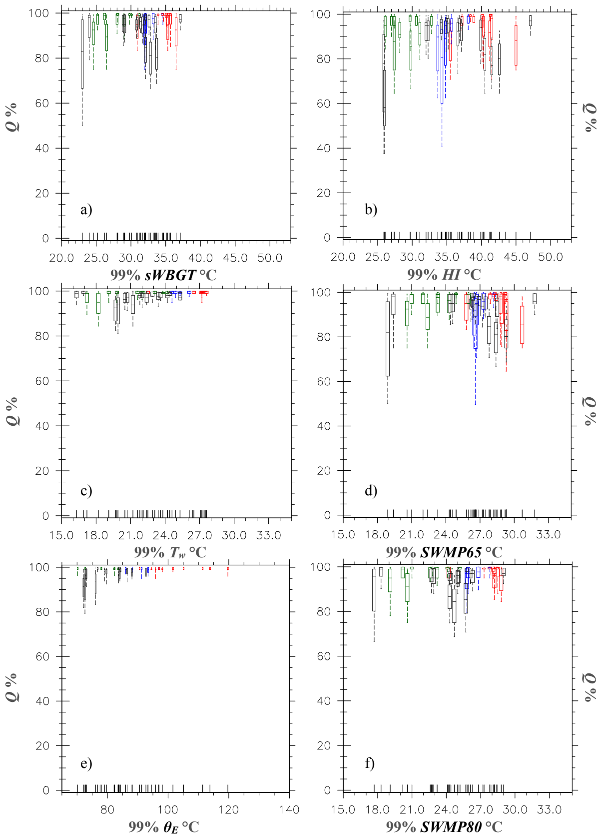


**Figure 7.** 1901–2010 CLM4.5 forced by CRUNCEP regional joint distribution box plots of $Q$ climatological percent from the 99th percentile. **(a)** Q_g_sWBGT, **(b)** Q_g_HI, **(c)** Q_g_$T_w$, **(d)** Q_g_SWMP65, **(e)** Q_g_$\theta_E$, **(f)** Q_g_SWMP80. Colors are same as in Fig. 4.